



Publicly Accessible Penn Dissertations


1-1-2015

Homologous Recombination-Directed Mechanisms of Alternative Lengthening of Telomeres

Nam Woo Cho

University of Pennsylvania, namwcho@mail.med.upenn.edu

Follow this and additional works at: <http://repository.upenn.edu/edissertations>

 Part of the [Cell Biology Commons](#), and the [Molecular Biology Commons](#)

Recommended Citation

Cho, Nam Woo, "Homologous Recombination-Directed Mechanisms of Alternative Lengthening of Telomeres" (2015). *Publicly Accessible Penn Dissertations*. 1655.

<http://repository.upenn.edu/edissertations/1655>

This paper is posted at ScholarlyCommons. <http://repository.upenn.edu/edissertations/1655>

For more information, please contact libraryrepository@pobox.upenn.edu.

Homologous Recombination-Directed Mechanisms of Alternative Lengthening of Telomeres

Abstract

Telomere length maintenance is a requisite feature of cellular immortalization and a hallmark of human cancer. While most human cancers express telomerase activity, ~10%-15% employ a recombination-dependent telomere maintenance pathway known as alternative lengthening of telomeres (ALT) that is characterized by multi-telomere clusters and associated promyelocytic leukemia protein bodies. However, the mechanisms that govern the lengthening process are poorly understood. Here, we show that a DNA double-strand break (DSB) response at ALT telomeres triggers long-range movement and clustering between chromosome termini, resulting in homology-directed telomere synthesis. Damaged telomeres initiate increased random surveillance of nuclear space before displaying rapid directional movement and association with recipient telomeres over micron-range distances. This phenomenon required Rad51 and the Hop2-Mnd1 heterodimer, which are essential for homologous chromosome synapsis during meiosis. Recruitment of Rad51 and Hop2 to damaged telomeres was dependent on ATR and Chk1 signaling. These findings implicate a specialized homology searching mechanism in ALT-dependent telomere maintenance and provide a molecular basis underlying the preference for recombination between nonsister telomeres during ALT.

Degree Type

Dissertation

Degree Name

Doctor of Philosophy (PhD)

Graduate Group

Cell & Molecular Biology

First Advisor

Roger A. Greenberg

Second Advisor

Michael A. Lampson

Keywords

Alternative Lengthening of Telomeres, Homologous recombination

Subject Categories

Cell Biology | Molecular Biology

HOMOLOGOUS RECOMBINATION-DIRECTED MECHANISMS OF
ALTERNATIVE LENGTHENING OF TELOMERES

Nam Woo Cho

A DISSERTATION

in

Cell and Molecular Biology

Presented to the Faculties of the University of Pennsylvania

in

Partial Fulfillment of the Requirements for the
Degree of Doctor of Philosophy

2015

Supervisor of Dissertation

Roger A. Greenberg, M.D. Ph.D., Associate Professor of Cancer Biology

Graduate Group Chairperson

Daniel S. Kessler, Ph.D., Associate Professor of Cell and Developmental Biology

Dissertation Committee:

Michael Lampson, Ph.D., Associate Professor of Biology

F. Bradley Johnson, M.D. Ph.D., Associate Professor of Pathology and Laboratory
Medicine

Ronen Marmorstein, Ph.D., Professor of Biochemistry and Biophysics

David Roth, M.D. Ph.D., Professor of Pathology and Laboratory Medicine

Eric Witze, Ph.D., Assistant Professor of Cancer Biology

HOMOLOGOUS RECOMBINATION-DIRECTED MECHANISMS OF
ALTERNATIVE LENGTHENING OF TELOMERES

COPYRIGHT

2015

Nam Woo Cho

This work is licensed under the
Creative Commons Attribution-
NonCommercial-ShareAlike 3.0
License

To view a copy of this license, visit

<http://creativecommons.org/licenses/by-nc-sa/2.0/>

Acknowledgement

I would like to extend my sincerest gratitude for those who made the work contained within this thesis possible. Roger has been the best mentor and a source of constant learning that I hoped for, walking with me through the entire journey. I also thank Robert, Niraj, Qinqin, Shane and Karl, the lab members on whom I constantly relied until the finish line. I thank Mike, who has provided instrumental help and guidance in visualization and analysis of telomeres. Last but not least, I thank my family and friends. The very last words of acknowledgement, I saved for my wife Eun Ji for her understanding and constant love throughout the past few years.

ABSTRACT

HOMOLOGOUS RECOMBINATION-DIRECTED MECHANISMS OF ALTERNATIVE LENGTHENING OF TELOMERES

Nam Woo Cho

Roger A. Greenberg

Telomere length maintenance is a requisite feature of cellular immortalization and a hallmark of human cancer. While most human cancers express telomerase activity, ~10%-15% employ a recombination-dependent telomere maintenance pathway known as alternative lengthening of telomeres (ALT) that is characterized by multi-telomere clusters and associated promyelocytic leukemia protein bodies. However, the mechanisms that govern the lengthening process are poorly understood. Here, we show that a DNA double-strand break (DSB) response at ALT telomeres triggers long-range movement and clustering between chromosome termini, resulting in homology-directed telomere synthesis. Damaged telomeres initiate increased random surveillance of nuclear space before displaying rapid directional movement and association with recipient telomeres over micron-range distances. This phenomenon required Rad51 and the Hop2-Mnd1 heterodimer, which are essential for homologous chromosome synapsis during meiosis. Recruitment of Rad51 and Hop2 to damaged telomeres was dependent on ATR and Chk1 signaling. These findings implicate a specialized homology searching

mechanism in ALT-dependent telomere maintenance and provide a molecular basis underlying the preference for recombination between nonsister telomeres during ALT.

Table of Contents

ACKNOWLEDGEMENT	III
ABSTRACT	IV
LIST OF FIGURES	VIII
CHAPTER 1. INTRODUCTION	1
I. Homologous recombination safeguards genome integrity	1
II. DNA damage responses at the telomere	2
III. Mechanisms of telomere length maintenance	3
IV. Hallmarks of ALT	4
V. Substrates of recombination of ALT telomeres	6
VI. Current gap in knowledge and potential mechanisms of ALT recombination	7
CHAPTER 2. INTERCHROMOSOMAL HOMOLOGY SEARCHES DRIVE DIRECTIONAL ALT TELOMERE MOVEMENT AND SYNAPSIS	10
I. Introduction	10
II. Telomere Double-Strand Breaks Increase the Hallmarks of ALT Recombination	11
III. Double-Strand Breaks Initiate Directional ALT Telomere Movement and Clustering	14
IV. Homologous Recombination Predominates at ALT Telomere DSBs	18
V. Rad51 and the HR Machinery Control Directional ALT Telomere Movement and Clustering	19
V. Hop2-Mnd1 Regulate ALT Telomere Movement and Recombination	21
VII. Discussion	23
VIII. Experimental Procedures	25

CHAPTER 3. REGULATION OF ALT TELOMERE RECOMBINATION BY THE ATR-CHK1 KINASE PATHWAY	35
I. Introduction	35
II. Inhibition of ATR and Chk1 activity disrupts HR factor localization at ALT telomeres	36
III. Inhibition of ATR and Chk1 results in genome-wide DNA fragmentation	37
IV. Limiting replication-dependent fork breakage partially rescues the loss of Rad51 and Hop2 from ALT telomeres	39
V. Abrogation of Hop2 expression by CRISPR/Cas9 disrupts ALT activity	40
VI. Discussion	41
VII. Experimental Procedures.....	43
CHAPTER 4. CONCLUSIONS AND FUTURE DIRECTIONS	46
FIGURES.....	54
BIBLIOGRAPHY.....	99

List of Figures

Figure 1. TRF1-FokI DSBs Promote Telomeric Clustering in ALT Cells

Figure 2. TRF1-FokI Induced Clustering Occurs Specifically in ALT Cells

Figure 3. TRF1-FokI DSBs Promote ALT Activity

Figure 4. TRF1-FokI DSBs Promote ALT Activity

Figure 5. ALT Telomere DSBs Rapidly Associate by Long Range, Directional Movement

Figure 6. Damage-dependent Chromatin Movement in ALT is Telomere Specific

Figure 7. Homologous Recombination Predominates at ALT Telomere DSBs

Figure 8. Increased Single-stranded Telomeric Signal is Largely from Telomeric Overhangs

Figure 9. Rad51 Promotes Diffusive and Directed ALT Telomere Movement

Figure 10. Rad51 Guides ALT Telomere Movement and Clustering

Figure 11. Hop2-Mnd1 Regulate Telomere Clustering and Recombination in ALT

Figure 12. Hop2-Mnd1 Regulates Telomere Clustering and Recombination in ALT

Figure 13. Model for a Specialized Homology Search Mechanism that drives ALT Telomere Recombination

Figure 14. Hop2-Mnd1 Regulates Telomere Clustering and Recombination in ALT

Figure 15. Hop2 localization to telomeres is disrupted upon ATR or Chk1 inhibition

Figure 16. ATR and Chk1 inhibition reduces Rad51, but not RPA, localization to ALT telomeres

Figure 17. Genome fragmentation occurs following ATR or Chk1 inhibition

Figure 18. γ H2Ax is increased following ATR or Chk1 inhibition in LM216^{ALT} and LM216^{TEL} cells

Figure 19. Roscovitine and Mus81 knockdown rescues the effects of ATRi and Chk1i

Figure 20. CRISPR-Cas9 mediated deletion of Hop2 suppress ALT phenotypes

Movie 1. Live cell imaging of telomeres after DSB induction demonstrates movement and clustering.

Movie 2. Live cell imaging of telomeres in the absence of DSBs.

Movie 3. Example of spontaneous telomere clustering.

Movie 4. Live cell imaging of mCherry-TRF1FokI foci and interconnecting GFP-Rad51 filaments in a VA13 cell.

Movie 5. Live cell imaging of telomeres in U2OS transfected with control siRNA.

Movie 6. Live cell imaging of telomeres in U2OS transfected with siRNA targeted to Rad51 demonstrates reduced movement.

Movie 7. Live cell imaging of telomeres in U2OS transfected with siRNA targeted to Hop2 demonstrates reduced movement.

CHAPTER 1. Introduction

I. Homologous recombination safeguards genome integrity

Homologous recombination (HR) is an evolutionarily conserved mechanism of DNA repair that is essential to genome integrity in meiotic and mitotic cells (Mazon et al., 2010; Moynahan and Jasin, 2010). In particular, this form of DNA repair as a response to double-strand breaks (DSBs) requires a highly coordinated process that culminates in an accurate search for and copying of a template DNA with sequence homology to the broken DNA. One of the critical early steps in this pathway is nucleolytic resection of DNA ends to generate 3' single-stranded DNA (ssDNA) overhangs—this precludes ligation repair by the potentially more mutagenic non-homologous end-joining (NHEJ) pathway (Symington, 2014). Instead, the ssDNA is rapidly bound by replication protein A (RPA), which is subsequently replaced by the Rad51 recombinase. Rad51-coated ssDNA nucleoprotein filament then initiates a search for homologous sequences (Qi et al., 2015). Successful capture of homology entails base pairing between invading single stranded DNA with the complementary strand of duplex DNA, forming a displacement loop (D-loop). Subsequent close association of the homologous strands (synapsis) and extension by DNA polymerases enables template-directed DNA repair.

HR-mediated DNA repair mechanisms are largely cell-cycle restricted to S and G2 phases in mitotic cells in eukaryotes when a sister chromosome is present and resection-promoting nucleases are more active (Aylon et al., 2004; Huertas et al., 2008;

Ira et al., 2004). HR between sister chromatids, rather than homologous chromosomes, is thought to be the vastly preferred mechanism of HR in mitotic cells (Johnson and Jasin, 2000). Conversely, meiotic HR is not limited to sister chromatid recombination, but occurs extensively between sequences on homologous chromosomes (Neale and Keeney, 2006). Meiotic recombination involves a lineage-restricted, programmatic form of HR that is initiated by Spo11 induced DSBs and culminates in synapsis of distant homologous loci. This process requires Rad51 and Dmc1 as well as the heterodimeric Hop2-Mnd1 proteins, which promote Rad51- and Dmc1-dependent D-loop formation in vitro and are epistatic to these RecA homologs during meiosis in yeast and in mammalian organisms (Bishop, 1994; Chi et al., 2007; Petukhova et al., 2003; Pezza et al., 2007). Thus, 3-dimensional genome organization during physiologic meiotic recombination is intimately linked to the repair mechanisms that execute homology searches between non-sister, homologous chromosomes.

II. DNA damage responses at the telomere

A region of the genome that is particularly susceptible to DSB repair mechanisms is the telomere, a stretch of repetitive homologous DNA sequences (TTAGGG in vertebrates) that encase each eukaryotic chromosome termini. By virtue of their position at the end of linear chromosomes, telomeres are potentially recognized as DSBs in the absence of protective mechanisms such as T-loop formation and presence a multi-protein complex termed the Shelterin complex (de Lange, 2005; Griffith et al., 1999). Depletion of one or more of the components of the Shelterin complex predisposes the telomere to

specific pathways of DNA repair—NHEJ dependent telomere fusions occur in the absence of TRF2, for instance, and HR can proceed in the setting of POT1 and Ku70/80 depletion (Sfeir and de Lange, 2012). These Shelterin-deficient or -free telomeres elicit a robust DNA damage response, and are referred to as “dysfunctional” or “deprotected” telomeres.

In addition, telomeres can shorten through a process known as the end replication problem. Due to the inability of the replication machinery to duplicate the region occupied by the RNA primer on the lagging strand, each cell cycle results in telomere shortening of about 50-150 base pairs (Martens et al., 2000). Cells that have gone through a sufficient number of divisions to reach a telomere length of 1-2 kilobases will undergo senescence. Those that can bypass senescence will most likely die from excessive damage responses at the telomere, especially during mitosis, in a phase known as crisis (Hayashi et al., 2015). Thus, telomeres represent a critical location in the genome at which DNA damage responses are normally appropriately suppressed in order to safeguard genome integrity and cellular viability.

III. Mechanisms of telomere length maintenance

Cells that continuously divide must avert cell death from telomere shortening and deprotection. The first mechanism is activation of a reverse transcriptase enzyme complex known as telomerase, and this occurs in 80-85% of all cancers as well as in normal germ and stem cells (Greider and Blackburn, 1985). The telomerase enzyme

complex uses a non-coding RNA template to processively add telomeric repeats to the ends of chromosomes. The second mechanism of telomere elongation, occurring in 10-15% of human cancers, is termed the Alternative Lengthening of Telomeres (ALT). ALT is defined as telomere maintenance occurring in the absence of telomerase activity. In spite of the potential sequelae of aberrant DNA repair reactions at the telomere, cells that utilize ALT rely on template directed DNA recombination to maintain or lengthen their telomeres (Dunham et al., 2000). In cancers, telomerase reactivation and ALT each occur exclusively, even though each mechanism does not suppress the other given that ectopic expression of hTERT in ALT cells causes both length maintenance mechanisms to function concurrently (Cerone et al., 2001; Perrem et al., 2001). While anti-telomerase therapy has been explored, blocking telomerase may result in resistance by upregulation of ALT activity (Hu et al., 2012), highlighting the importance of understanding mechanisms in ALT to devise therapeutic approaches.

IV. Hallmarks of ALT

ALT is defined as a mechanism of telomere length maintenance in the absence of telomerase activity. However, while this definition is one of exclusion, ALT cells typically demonstrate several hallmarks that positively identify them. The first is the presence of ALT-associated Promyelocytic leukemia Bodies (APBs), which contain telomeric DNA within the PML nuclear bodies, along with telomere associated proteins, DNA repair proteins and chromatin modifying proteins (Yeager et al., 1999). Since DNA damage repair proteins can be found in PML bodies within non-ALT cells, the presence

of telomeric DNA is an exclusive finding in ALT-utilizing cells (Dellaire and Bazett-Jones, 2004).

The presence of APBs correlates with telomere maintenance by ALT. Disruption of APBs by depletion of PML itself or components of the Mre11/Rad50/Nbs1 (MRN) complex suppresses telomere length maintenance in ALT cells (Jiang et al., 2005; Zhong et al., 2007). Furthermore, bromodeoxyuridine (BrdU) accumulation can occur within APBs in non-S phase cells, indicating that active DNA synthesis is occurring likely as a part of a DNA repair process as opposed to normal DNA replication (Nabetani et al., 2004). Importantly, APBs are often strikingly large in size—they can reach sizes up to several microns—and can contain multiple telomeric material from different chromosomes as well as extrachromosomal telomeric fragments (Draskovic et al., 2009; Fasching et al., 2007; Komosa et al., 2015). This is critical for ALT-sustaining recombination reactions that require a donor and a recipient molecule for the formation of the D-loop. A high local concentration of DNA repair factors such as RPA32 and Rad51 among a host of other factors likely facilitates recombination.

ALT has also been found to occur in cells lacking APBs (Cerone et al., 2005; Fasching et al., 2005; Marciniak et al., 2005). Interestingly, some of these cell lines display arrays of non-telomeric and telomeric amplifcons arranged in tandem. This is analogous to ALT in *Saccharomyces cerevisiae*, where type I survivors show amplifications of both telomeric G-rich DNA and subtelomeric Y' repeat elements, and type II survivors demonstrate amplifications of only the telomeric G-rich repeats.

Mechanisms governing these potential distinct pathways within ALT have not been investigated in detail.

The other hallmarks of ALT include long and heterogeneous telomere lengths, telomere sister chromatid exchanges (T-SCEs), and the presence of extrachromosomal telomeric repeats (ECTRs) such as double-stranded T-circles, largely single stranded c-circles and linear DNA (Cesare and Griffith, 2004; Henson et al., 2009). These hallmarks are likely generated from the possible recombination reactions in ALT, which will be discussed next.

V. Substrates of recombination of ALT telomeres

Due to the repetitive nature of telomeres, recombination at telomeres can theoretically occur with a variety of substrates and not necessitate a sister strand, which is normally the vastly preferred substrate for HR (Johnson and Jasin, 2000). These substrates, which are available even outside of S/G2 phases of the cell cycle, include telomeres from another chromosome, and ECTRs such as T-circles or C-circles. Interchromosomal telomeric recombination is evidenced in the initial study which characterized ALT, demonstrating interchromosomal copying of a telomere-integrated neomycin resistance tag (Dunham et al., 2000). Furthermore, interchromosomal telomeric bridges composed of telomeric sequences can be found in metaphase chromosome spreads of ALT cells (Draskovic et al., 2009). While a rolling-circle amplification

mechanism such as those demonstrated in yeast is a possibility (Natarajan and McEachern, 2002), this has not yet been shown in human ALT cells.

Another possible substrate is the sister telomere in the S/G2 phases of the cell cycle. This activity is suggested by the presence of T-SCEs, which are post-replicative exchanges in G- or C-rich telomeric sequence resulting in a double signal at a particular chromosome end (Bailey et al., 2004; Londono-Vallejo et al., 2004). T-SCEs are generally elevated in ALT cells, although whether these exchange events actually lead to telomere elongation or merely represent increased recombination activity at ALT telomeres remains to be sorted out. Furthermore, exchange events can often occur at only one of the two sister chromatids, whereas a normal exchange between sister chromatids would result in double signals at both sister chromatids (Conomos et al., 2014). It is likely that these one-sided exchanges represent recombination with a non-sister substrate.

VI. Current gap in knowledge and potential mechanisms of ALT recombination

A mechanistic understanding of how ALT telomeres recombine is needed. A plausible model follows a classical model for HR. In this model, the initial step of recombination involves generation of a 3' overhang, which if at the end of the chromosome, is composed of the G-rich sequence. This overhang could be potentially generated by various nucleases such as Mre11, Exo1, CTIP and Dna2. Alternatively, they may be unmasked during the normal progression of replication through the telomere. This overhang should subsequently invade into homologous double-stranded substrate

telomere and form a D-loop. It is unclear, however, how this search for homology occurs. What are the factors that regulate the initial resection and homology search process?

Once the D-loop is formed, several reactions can proceed depending on the nature of the invading molecule. If both sides of the break contain homology to the intact substrate, repair could occur by formation of a double Holliday Junction leading to gene conversion (GC), or by synthesis-dependent strand annealing (SDSA). Gene conversion is the predominant outcome for breaks at the vast majority of DSBs in somatic cells. However, if the homology is one-sided or if the break is one-ended, repair can proceed by a process that may be similar to break-induced replication (BIR) as described in yeast (McEachern and Haber, 2006). This mechanism is particularly attractive to explain ALT recombination since the repair would proceed by continuous leading and lagging strand synthesis for greater than 100 kilobases, resulting in net elongation of the invading strand (Donnianni and Symington, 2013).

While Rad51 is predicted to be important for the critical strand invasion process, it is notable that BIR in yeast can occur in a Rad51-dependent and –independent manner (Malkova et al., 1996). Furthermore, the two types of yeast survivors lacking telomerase can arise in the setting of Rad51 deletion (type II, telomeric amplification only) and in the setting of Rad50 deletion (type I, telomeric and subtelomeric amplification). It is unclear whether these types of pathways exist in human ALT cells and to what extent these potential mechanisms contribute to ALT telomere maintenance and survival.

Lastly, it is unknown what roles the major DNA polymerases play in telomeric DNA synthesis during ALT recombination. Pol32, a subunit of the delta polymerase complex, is important for yeast BIR (Lydeard et al., 2007) and its human ortholog PolD3 has been reported to be important for BIR in mammalian cells (Costantino et al., 2014). Given these findings, it would be instructive to test the role of PolD3 in ALT telomere synthesis.

CHAPTER 2. Interchromosomal Homology Searches Drive Directional ALT Telomere Movement and Synapsis

I. Introduction

A subset of ALT telomeres coalesces into characteristic ALT-associated PML Body (APB) structures that display multiple telomeres from different chromosomes in association with PML (Draskovic et al., 2009; Jegou et al., 2009; Molenaar et al., 2003; Yeager et al., 1999). These multi-telomere bodies are thought to be sites of homology-directed telomere synthesis (Nabetani et al., 2004). While the nature of the initiating stimulus for ALT recombination is unclear, one plausible mechanism is that DSB responses at a subset of ALT telomeres would represent a seminal event that initiates the search and capture of distant homologous DNA. Pairing and recombination between telomeres from different chromosomes during ALT would necessitate long range telomere movement.

Damage dependent increases in local DNA mobility have been documented in both prokaryotes and eukaryotes, which may suggest that increased movement of broken chromosomes assists in repair of these loci (Aten et al., 2004; Chen et al., 2013; Dimitrova et al., 2008; Dion et al., 2012; Krawczyk et al., 2012; Mine-Hattab and Rothstein, 2012; Roukos et al., 2013). Interestingly, DNA damaging agents increase the prevalence of APBs in ALT cells, and a subset of ALT telomeres accumulates DNA repair proteins (Cesare et al., 2009; Fasching et al., 2007). Furthermore, while the

majority of telomeres in ALT-positive osteosarcoma U2OS cells display relatively slow mobility confined to a radius of less than 0.5 μ m, up to 15% of telomeres show unusually high mobility (Jegou et al., 2009; Molenaar et al., 2003). Yet, how increased mobility would facilitate efficient associations between damaged DNA and homologous genomic regions remains enigmatic, as are molecular events underlying such migration of DNA across the nucleoplasm lacking canonical structures of cellular transport such as microtubules.

This section provides direct evidence that telomeric DSB responses drive inter-telomere associations in the context of ALT telomeric chromatin. Strikingly, increased ALT telomere mobility culminated in rapid and directional movement over micron distances toward a recipient telomere, providing a real-time cellular visualization of homology search and synapsis in a mammalian cell nucleus. This process required the HR machinery including Rad51, which could be directly visualized in between recombining telomeres, representing a putative recombination intermediate. Moreover, these studies reveal that ALT cells commandeer proteins critical for meiotic recombination searching mechanisms, providing insights into this specialized form of HR-driven telomere maintenance.

II. Telomere Double-Strand Breaks Increase the Hallmarks of ALT Recombination

Telomeric chromatin is bound by a set of proteins that recognize double and single stranded repetitive telomere DNA, termed the Shelterin complex (Cesare and

Karlseder, 2012; Palm and de Lange, 2008). Fusion of the telomere repeat binding factor, TRF1, to the FokI nuclease catalytic domain targets DSBs specifically at telomeres in both telomerase positive and ALT cells, leading to a robust induction of DSB responses that extend hundreds of kilobases into subtelomeric chromatin (Tang et al., 2013). Further characterization of TRF1-FokI expression revealed a DSB response equivalent to approximately 1-2 Gy ionizing radiation in U2OS cells as assessed by western blot using antibodies to γ H2AX, and phosphorylated-ATM (Figures 1A and B). Notably, Chk2 phosphorylation was not increased to similar levels as phospho-ATM, consistent with prior reports that telomere damage signals are not efficiently transmitted to some ATM substrates (Cesare et al., 2013). Despite reduced transmission of ATM phosphorylation to Chk2, TRF1-FokI expression resulted in a nearly 2-fold increase in cells in the G2 phase of the cell cycle, consistent with the induction of a G2/M checkpoint (Figure 2A).

Interestingly, TRF1-FokI expression resulted in up to 4-fold increases in average telomere foci size and reduced numbers of telomeres in each of 4 different ALT positive cell lines in comparison to cells expressing the nuclease inactive TRF1-FokI D450A mutant (Figures 1C, 1D and 2B). Telomere foci size increases did not occur in telomerase negative primary human IMR90 fibroblasts or 4 different telomerase positive cell lines. Telomere length difference between ALT and telomerase positive cells was not sufficient to explain foci size increases, as TRF1-FokI expression did not significantly increase telomere foci size in the telomerase positive HeLa 1.3 cells (Figure 1D), which have a mean telomere length comparable to ALT cell lines.

Telomeres within these larger foci in ALT cells contain chromosomally attached telomeres. This is supported by the observation that metaphase chromosome spreads from D450A and WT TRF1-FokI were not appreciably different with respect to the percentage of chromosome ends displaying telomeric signal, and by the presence of subtelomeric fluorescence in situ hybridization (FISH) signals or subtelomeric lac operator transgene repeats juxtaposing telomeres in interphase U2OS cells (Shanbhag et al., 2010) (Figures 2C-E). Furthermore, expression of TRF1-FokI increased the percentage of multiple subtelomeric FISH signals accumulating at a telomere cluster (Figure 1E). These data are in agreement with previous reports that APB bodies contain chromosomally attached telomeres (Draskovic et al., 2009). However, they do not exclude the possibility that extra-chromosomal telomeric repeats (ECTRs), which increase in response to DNA damage, are also present in these large telomere bodies (Cesare and Griffith, 2004; Fasching et al., 2007).

These findings suggest that DSB responses at ALT telomeric chromatin provide the initiating stimulus for telomere clustering. Consistent with this expectation, TRF1-FokI expression induced multiple hallmarks of ALT recombination, including significant increases in telomeres associated with promyelocytic leukemia bodies (APBs) and telomere associated DNA synthesis as evidenced by incorporation of thymidine analog 5-ethynyl-2'-deoxyuridine (edU) in non S-phase cells (Figures 3A-D and Figure 4A). Similar findings were not detectable in telomerase positive cells. Expression of TRF1-FokI also increased c-circle formation, a specific indicator of ALT activity (Figures 4B-E) (Henson et al., 2009). Moreover, TRF1-FokI expression increased telomere length

heterogeneity by Terminal Restriction Fragment Analysis in 3 different ALT cell lines (Figure 3E). The increased heterogeneity could result from a combination of factors, including telomere cutting by TRF1-FokI, as well as ALT recombination associated length changes and ECTR generation. These telomeres were sensitive to digestion by Bal-31, an exonuclease that degrades duplex DNA from both 3' and 5' ends, indicating that the longer telomere fragments observable following TRF1-FokI WT expression were not a consequence of telomere-telomere end joining (Figure 3F).

III. Double-Strand Breaks Initiate Directional ALT Telomere Movement and Clustering

The presence of intense ALT-like telomere clusters suggests that DSB responses initiate a homology search process, followed by synapsis and recombination between distant telomeres. To directly test this hypothesis, we visualized telomere movement using an inducible mCherryTRF1-FokI fused to a modified estradiol receptor and destabilization domain, which allowed small molecule induction by administration of 4-hydroxytamoxifen and Shield1 ligand (Figure 5A). Following a 1-hour induction period, TRF1-FokI expressing cells were monitored over the following hour by capturing confocal z stacks of the entire nucleus every 2 minutes. Telomere foci were tracked in the z-projected plane, and a registration process (Thevenaz et al., 1998) assisted normalization for cellular movement.

Strikingly, telomeres in TRF1-FokI WT expressing cells demonstrated increased mobility and an average of 7 telomere-telomere clustering events per hour between foci separated by up to 5 μ m (Figures 5B, C, E, F and Movie 1). Telomere clustering and movement were greatly diminished in the nuclease inactive D450A mutant or in cells expressing mCherry-TRF1 (Figures 5B-D and Movies 2 and 3). Importantly, less frequent instances of clustering were observed at mCherry-D450A and TRF1 containing telomeres, consistent with a previous report of an association of two telomeres in an unperturbed U2OS cell (Molenaar et al., 2003). TRF1-FokI induced DSBs at ALT telomeres greatly increase the frequency of telomere associations that normally occur in these cells.

To determine if DSBs at other regions of the genome in ALT cells would demonstrate similar movement and clustering as those observed at telomeres, we monitored targeted and random DSB positions at non-telomeric locations. Fusion of FokI to the Lac repressor (mCherryLacIFokI) enables efficient visualization of DSB responses at lac operator repeat sequences integrated into chromosome 1p36 (Shanbhag et al., 2010). mCherryLacIFokI DSBs did not display large increases in mobility at this locus in U2OS cells (Figures 6A and B). GFP-53BP1 movement and clustering was also minimal at most ionizing radiation induced foci during time lapse imaging in U2OS cells (Figure 6C). Conversely, telomeric DSBs moved coordinately with the sub-telomeric LacO locus in cells expressing both GFP-LacI and mCherryTRF1-FokI (Figure 6D). The lack of substantial DSB movement at non-telomeric regions of the genome is consistent with

reports that ALT cells display elevated recombination at telomeres, but not elsewhere in the genome (Bechter et al., 2003; Dunham et al., 2000).

Importantly, the robust increase in ALT telomere movement allowed a quantitative analysis of this type of chromatin movement. Telomere tracks were subjected to a mean squared displacement (MSD) analysis, which plots the average squared displacements at each time interval, given by equation $MSD = \langle (x(t+\Delta t) - x(t))^2 \rangle$, where x is the position of the focus and t is time. The MSD trajectories were then fitted to a single exponential time dependence diffusion model described by $MSD = \Gamma t^\alpha$ where Γ is a generalized coefficient, and α is a time dependence coefficient which can be used to determine the type of motion. For $\alpha \sim 1$, the particle is undergoing normal diffusion, and $\alpha < 1$ represents sub-diffusion, also known as anomalous diffusion. Subdiffusive target searches in cells can result from molecular crowding of the nucleus and cytoplasm (Guigas and Weiss, 2008). Finally, $\alpha \geq 2$ represents an exponential dependence on time that indicates that the particle is moving in a directed manner, an example of which is active cellular transport.

A comparison of averaged MSD trajectories for all telomeres in TRF1-FokI WT or D450A expressing U2OS cells revealed that $\alpha = 0.8$ for WT and $\alpha = 0.7$ for D450A, both characteristic of subdiffusive motion (Figure 5D). The Γ coefficient, which describes the magnitude of the behavior characterized by α , was greater for WT than for D450A, with values of $4.7 \times 10^{-2} \mu\text{m}^2 \text{s}^{-\alpha}$ and $3.3 \times 10^{-2} \mu\text{m}^2 \text{s}^{-\alpha}$ respectively. Calculation of time-dependent diffusion coefficient $D(t) = MSD/t = \Gamma t^{\alpha-1}$ showed that the diffusion coefficient decreases linearly with time with a slope of $\alpha-1$ when plotted on a log-log

scale, consistent with subdiffusive motion (Saxton, 2007). For D450A, $D(t)$ at 15 minutes was $1.4 \times 10^{-2} \mu\text{m}^2 \text{min}^{-1}$, consistent with values for normal U2OS telomeres (Molenaar et al., 2003), and decreased to $0.9 \times 10^{-2} \mu\text{m}^2 \text{min}^{-1}$ at the end of the observation period (Figure 6A). For WT, however, $D(t)$ was consistently elevated at $2.6 \times 10^{-2} \mu\text{m}^2 \text{min}^{-1}$ and $1.9 \times 10^{-2} \mu\text{m}^2 \text{min}^{-1}$ at 15 minutes and 60 minutes respectively (Figure 6E). These results indicate that damaged telomeres move faster and roam a larger nuclear territory.

While all telomeres considered in sum demonstrated diffusive movement, it was readily apparent from imaging experiments that faster, “incoming” telomeres displayed a striking long-range directional movement prior to association with a comparatively slow-moving “recipient” telomere (Figure 5B, E and Movie 1). For a quantitative analysis of this observation, mobility data from telomeres that merged into a recipient telomere was isolated. The terminal behavior of such telomeres was characterized by MSD analysis of the last 10 timepoints of each track, with the ultimate timepoint representing the merge event. The shape of the resulting MSD trajectory suggested an initial, increased diffusive movement for Δt of up to 10 minutes, followed by a transition to directed movement at large Δt (Figure 5G). This change in behavior was clearly visualized on a log-log plot. The α coefficient for the initial portion of the clustering telomere trajectory was 0.9 suggestive of diffusive motion, but between Δt of 12-18 minutes, there was a clear transition of α to ~ 2.3 , indicative of directed movement (Figure 5H).

The average displacement of telomeres during this directed phase was $\sim 1.3 \mu\text{m}$ with up to $4\text{-}5 \mu\text{m}$ observed for some tracks (Figure 5E, F). Following the clustering event, the merged telomere foci demonstrated reduced movement (Figure 3I), suggesting

the searching process that underlies directional movement had concluded. Interestingly, the less mobile, “recipient” telomere was associated with PML in 85% of clustering events (Figure 6F). This supports a model in which PML promotes clustering and recombination of telomeres within APBs (Chung et al., 2011; Draskovic et al., 2009).

To further address whether the driving force behind ALT telomere movement is a DSB response, spontaneous telomere clustering events in mcherryTRF1 expressing VA13 cells were quantified with respect to colocalization of GFP-53BP1 as a marker of DSBs. Greater than 60% of clustering telomeres accumulated GFP-53BP1 prior to association, while 15% of all telomeres were associated with GFP-53BP1. This indicates that telomere movement and clustering is closely correlated with a local DNA damage response (Figure 6G, H).

IV. Homologous Recombination Predominates at ALT Telomere DSBs

The presence of random surveillance followed by directional DSB induced telomere movement could be a consequence of a homology search and capture between distant telomeres. Resection of telomeric ends would be a critical determinant of this pathway choice. RPA localization was assessed at telomeres in cells expressing TRF1-FokI in ALT and telomerase positive cells. HeLa 1.3 did not significantly accumulate RPA at telomeres. Conversely, telomeres in both U2OS and VA13 cells were associated with RPA at baseline, which further increased in the presence of TRF1-FokI (Figures 7A, B). Furthermore, expression of TRF1-FokI in U2OS cells resulted in an increase in

single-stranded telomeres as assessed by electrophoresis and hybridization of telomeric probes under native conditions (Figure 7C). The increased ssDNA was largely derived from telomeric overhangs, since the native single stranded telomeric signal was reduced following treatment with ExoI ssDNA exonuclease (Figure 8A).

Consistent with the observed increases in resection, homologous recombination proteins BRCA1 and Rad51 were present directly overlying 20-60% of telomeres in ALT cells and only 5-15% of telomeres in telomerase positive cells after TRF1-FokI DSB induction (Figures 7D and E). 53BP1 immunofluorescence juxtaposed BRCA1 in both ALT and telomerase positive cells, consistent with known differences of BRCA1 and 53BP1 chromatin localization adjacent to DSBs (Figures 7D and 8B) (Chapman et al., 2012; Tang et al., 2013).

V. Rad51 and the HR Machinery Control Directional ALT Telomere Movement and Clustering

These observations raise the possibility of homology directed telomere movement, analogous to the reported Rad51 dependency for DSB movement that occurs during homology searches in yeast (Dion et al., 2012; Kalocsay et al., 2009; Mine-Hattab and Rothstein, 2012; Oza et al., 2009). To test this hypothesis, TRF1-FokI induced telomere clustering was quantified following siRNA-targeted depletion of factors involved in either HR or NHEJ (Figure 9A and 10A). Knockdown of NBS1 and SMC5 reduced telomere clustering in accord with their known involvement in ALT (Potts and

Yu, 2007; Wu et al., 2003; Zhong et al., 2007). Similar reductions were observed in cells following knockdown of either BRCA2 or Rad51, but not 53BP1 (Figure 9A) (Jiang et al., 2007). Interestingly, ALT telomere clustering was independent of BRCA1, consistent with the HR competency of cells that exhibit extensive resection as a consequence of 53BP1 deficiency (Bouwman et al., 2010; Bunting et al., 2010).

Rad51 molecules nucleate onto RPA-coated ssDNA forming a dynamic nucleoprotein filament which mediates the presynaptic search for homology (Renkawitz et al., 2014). Remarkably, expression of GFP-tagged Rad51 in VA13 cells allowed visualization of GFP-Rad51 filaments that originate specifically at telomeres and extended to distant telomeres (Figure 9B). Live cell imaging revealed that clustering could proceed by rapid shortening of the GFP-Rad51 filament with synchronous directional movement of the incoming telomere (Figures 9C and Movie 4). Of 35 clustering events in cells in which a bridging filament formation was evident, 86% showed Rad51 localization. Rad51 filament could be directly visualized between recombining telomeres in approximately 46% of cases in which Rad51 was observable at telomeres (Figure 10B).

MSD analysis revealed that Rad51 knockdown restricted telomere mobility as well as telomere clustering events that occur as a result of directed movement (Figures 9D, E and Movies 5 and 6). Interestingly, telomere clustering was decreased by expression of an ATPase defective dominant negative mutant of Rad51, K133R, which inhibits HR in mouse cells and has been reported to lock Rad51 filaments into an

extended conformation that cannot transition to a compressed filament (Figure 10C) (Robertson et al., 2009; Stark et al., 2002).

V. Hop2-Mnd1 Regulate ALT Telomere Movement and Recombination

TRF1-FokI DSB-induced telomere recombination resembles certain aspects of recombination between homologous chromosomes during meiosis, which is also initiated by programmed DSBs and requires RecA homologs Rad51 and Dmc1. The Hop2-Mnd1 heterodimer is necessary for Dmc1 and Rad51 dependent inter-homolog recombination *in vivo* during gametogenesis in yeast and in mice (Leu et al., 1998; Petukhova et al., 2003), and strongly stimulates Rad51 or Dmc1 dependent D-loop formation *in vitro* (Bugreev et al., 2014; Chi et al., 2007; Petukhova et al., 2005; Pezza et al., 2007). Moreover, Hop2-Mnd1 or Dmc1 mutant yeast and mice display epistasis with respect to meiotic chromosome inter-homolog synapsis. Hop2-Mnd1 binds double stranded DNA and induces rapid condensation of large stretches of DNA *in vitro*, consistent with its requirement for homolog synapsis (Pezza et al., 2010).

Hop2 protein was broadly expressed in all 16 different ALT cell lines and in telomerase positive cancer cell lines tested, with lower levels detected in primary human fibroblasts (Figures 11A and 12A-C). Endogenous Hop2 localized to approximately 10-20% of TRF1-FokI damaged telomeres in VA13 cells and at lower levels in the absence of TRF1-FokI (Figure 12E, F). GFP-Hop2 foci localized adjacent to telomeres in a subset of ALT cells and foci formation was completely ablated by an M110P point mutant

within the Hop2 Leucine Zipper domain (Figures 12G, H). This domain is required for homolog pairing and recombination, with the Leucine Zipper also being necessary for Hop2 dependent D-loop formation in vitro (Pezza et al., 2006). Hop2 or Mnd1 knockdown strongly reduced telomere clustering, mobility and directional movement to levels observed in D450A control cells (Figures 11B-D, 12D and Movie 7). Hop2-Mnd1 depletion did not affect Rad51 localization to damaged telomeres (Figure 12I), in agreement with established roles for the heterodimer in meiotic inter-homolog pairing but not Rad51 or Dmcl recruitment to Spo11 dependent DSBs (Petukhova et al., 2003).

To determine if these results would be recapitulated with respect to telomere clustering and recombination in ALT cell lines that did not express TRF1-FokI, several different ALT lines were quantified for spontaneous APB formation following knockdown of Hop2 or Mnd1 with 5 different targeting siRNAs (Figures 11E, F and 14A, B). Knockdown of either Hop2 or Mnd1 significantly reduced APB formation in each of these lines. The reduction in APBs could be fully rescued by stable expression of full length Hop2, which is resistant to a siRNA targeted to the 3'UTR (Figure 11G). To assess the impact of Hop2-Mnd1 on ALT telomere recombination, telomere chromatid exchanges were assessed by chromosome orientation-FISH (CO-FISH). Knockdown of Hop2 or Mnd1 reduced telomere chromatid exchanges by 50% or greater in ALT cells (Figures 11H, I and 14C). Collectively, these data reveal that the forces driving directional telomere movement are intimately connected to the mechanism of ALT telomere recombination based lengthening (Figure 13).

VII. Discussion

The phenomenon of DSB movement has been described in prokaryotes, yeast and also in mammalian cells within distinct experimental contexts (Aten et al., 2004; Dimitrova et al., 2008; Dion et al., 2012; Kalocsay et al., 2009; Lesterlin et al., 2013; Mine-Hattab and Rothstein, 2012; Oza et al., 2009; Roukos et al., 2013). Telomeres appear to be a particularly predisposed genomic location to DNA damage induced mobility increases. Diffusive movement of damaged telomeres in telomerase positive cells has been reported in several independent studies (Chen et al., 2013; Dimitrova et al., 2008). Notably, the NHEJ promoting factor 53BP1 was required for movement of deprotected mouse telomeres. However, TRF1-FokI induced directional ALT telomere mobility required HR factors and was independent of 53BP1, indicative of distinct mechanisms underlying telomere mobility in each case. Extensive end resection and more prominent accumulation of HR factors at damaged ALT telomeric chromatin likely contribute to these differences (Figure 13).

Expression of TRF1-FokI enabled quantitative characterization of an unanticipated type of chromatin movement. Damaged ALT telomeres initially roamed a larger nuclear territory at greater velocities than D450A controls, but notably, these movements culminated in rapid and directional movements of up to 5 μ m to synapse with a more stationary recipient telomere. These displacements were also much larger in magnitude and occurred over a longer time period than those of stochastic unidirectional “jumps” that could be seen in interphase chromatin (Levi et al., 2005). We note, however, that pre-selection of clustering tracks in our analysis introduces a bias of describing only

highly mobile particles. The analysis of directionality was limited to clustering telomeres, and this analysis does not preclude the possibility that a proportion of non-clustering telomeres could move directionally.

To our knowledge, directional ALT telomere movement provides the first example of real time visualization of homology searches and synapsis in mammalian cells. Given our data, we favor a model in which Rad51 nucleoprotein filaments interrogate surrounding nuclear space, leading to homology capture of a non-sister telomere and subsequent directional movement during synapsis (Figure 13). Interestingly, dynamic formation of long stretches of prokaryotic RecA coated filaments mediated rapid associations between DSBs and homologous genomic regions that are separated by 1.3 μ m (Lesterlin et al., 2013), which are similar to the distances of directional phase movement we describe for ALT telomeres. The reported structure of ssDNA filaments in association with RecA reveals an extended conformation that is stretched to \sim 1.5 fold longer B-form DNA (Chen et al., 2008). Thus, it is predicted that 1.3 μ m of nuclear space connecting non-sister telomeres could theoretically require only \sim 2.5kb of Rad51 ssDNA filament for directional movement, which is well within the length possible for ALT telomeres. Furthermore, as vertebrate telomeres contain extensive regions of homology consisting of TTAGGG repeats, in effect every chromosome is a “homolog” with respect to telomere recombination. This feature of primary telomere sequence would be predicted to increase the probability of recombination between different chromosomes, enabling successful capturing of distant homology on timescales similar to those observed in much smaller genomes. It should also be noted that not all recombining telomeres displayed

Rad51 foci, consistent with the presence of Rad51 independent mechanisms of ALT in type II survivors of telomerase deficiency in yeast (Chen et al., 2001).

Several obvious parallels exist between meiotic recombination and ALT. Both processes involve DSB responses to initiate recombination between homologous DNA sequences on non-sister chromatids. Hop2-Mnd1 uniquely contributes to chromosome pairing in meiotic recombination and ALT, but is not known to be important for sister chromatid recombination. Both constituents of this heterodimer are broadly expressed in ALT and telomerase positive cancers, yet appear to promote telomere recombination only in cells that use ALT. This may be a consequence of the known interaction of Hop2-Mnd1 with Rad51, which did not efficiently nucleate damaged telomeres in telomerase positive cells. It is also plausible that other factors related to the specific chromatin environment in ALT cells, such as the absence of ATRX and the association between ALT and defective histone chaperone activity (Heaphy et al., 2011; Lovejoy et al., 2012; O'Sullivan et al., 2014; Schwartzenuber et al., 2012), may promote inter-telomere recombination. Mechanistic studies into this process are warranted, as is the extent to which ALT recapitulates known mechanisms of meiotic recombination.

VIII. Experimental Procedures

Cell culture

Saos2 cells were grown in McCoy's 5A medium (Invitrogen) with 15% fetal bovine serum and 1% penn/strep. DLD cells were grown in RPMI (Invitrogen) with 10%

calf serum and 1% pen/strep. All other cell lines were grown in DMEM (Invitrogen) with 10% calf serum and 1% pen/strep. VA13 cell line refers to WI-38 VA-13 subline 2RA.

Plasmids, primers and siRNAs

Flag-TRF1-FokI fusion protein was cloned as previously described (Tang et al., 2013) into the HFUW lentiviral vector. The coding sequence for mCherry, the modified estrogen receptor (ER) and destabilization domains (DD) were PCR amplified and cloned in frame into the N terminus of TRF1-FokI. Rad51 cDNA was cloned into pEGFP-C1. The N terminal GFP tagged Hop2 expression vector was generated by PCR amplification and ligation of Hop2 cDNA corresponding to isoform 2 (RefSeq NM_016556.3) from ProQuest HeLa cDNA Library (Invitrogen). Hop2 M110P mutant was generated by site-directed mutagenesis.

The following primers were used for qRT-PCR: GAPDH (IDT, PrimeTime assay Hs.PT.39a.22214836), Hop2/PSMC3IP (IDT, PrimeTime assay Hs.PT.56a.40246325.g), Mnd1 (IDT, PrimeTime assay Hs.PT.56a.1133039).

The following siRNA sequences were used:

Luciferase, 5'-GCCAUUCUAUCCUCUAGAGGAUG-3'

Control, (Qiagen Allstars)

Rad51 #1, 5'-UGUAGCAUAUGCUCGAGCG-3'

Rad51 #2, 5'-CCAGAUCUGUCAUACGCUA-3'
Rad51 #3, 5'-UGGAGGGCUGACAGCUUCC-3'
NBS1 (Santa Cruz)
SMC5, 5'-GAAGCAAGAUGUUAUAGAA-3'
53BP1, 5'-UAUUACCGUCUCCUCGUUC-3'
CTIP, 5'-ACACACUCAUGGUGAUAAA-3'
BRCA1, 5'-AGAUAGUUCUACCAGUAAA-3'
BRCA2, 5'-GAAGAAUGCAGGUUUAU-3'
Hop2 #1, 5'-GCAGCUACCAAUCAUGUGA-3'
Hop2 #2, 5'-AAGAGAAGAUGUACGGCAA-3'
Hop2 #3, 5'-UCUGCUUAAAGGUGAAAGUAGCAGG-3'
Hop2 #4, 5'-UAAAUGUUAACCUCAAGCUACUGCA-3'
Mnd1 #1, 5'-GCUAACAGAUGGACUGAUA-3'

All siRNAs were transfected at 20nM, except for double transfections where each siRNA concentration was at 10nM, using Lipofectamine RNAiMAX (Invitrogen).

For Hop2 Mnd1 knockdown for APB quantification, knockdown was performed in series on day 1 and day 4 and cells were fixed on day 7.

Antibodies

The following antibodies were used: anti-53BP1 (rabbit, Novus), anti-BRCA1 D9 (mouse, Santa Cruz), anti- γ H2AX JBW301 (mouse, Millipore), anti-H2AX (rabbit,

Bethyl), anti-phosphoATM Ser-1981 (mouse, ECM Biosciences), anti-phosphoChk2 Thr-68 (Rabbit, Cell Signaling), anti-Flag M2 (mouse, Sigma), anti-PML (mouse, Santa Cruz), anti-Rad51 H-92 (mouse, Santa Cruz), anti-Hop2/PSMC3IP (rabbit, ProteinTech 11339-1-AP; rabbit, Novus NBP1-92301), anti-RPA2 (9H8, mouse, Novus).

Transfections and lentiviral transductions

Transient plasmid transfections were carried out with LipoD293 (Signagen), and siRNA transfections with Lipofectamine RNAiMax (Invitrogen) according to manufacturer's instructions. Concentrated TRF1-FokI lentivirus with polybrene (8ug/ml) diluted in media was added to cells at a minimum titer resulting in greater than 90% expression at 24 hours by immunofluorescence. Analyses were performed 16 hours after transfection of plasmids, and 48-72 hours after siRNA transfection. Analyses were performed 24 hours after transduction of cells with Flag-TRF1-FokI lentivirus.

Western blot

Cells were collected and lysed in RIPA buffer or for histone fractions, acid extracted. Proteins were resolved on a 4-12% bis-tris gel (Invitrogen). Transferred membranes were blocked in 5% milk and incubated with primary antibody overnight. For western blot following TRF1-FokI expression, cells were collected 24 hours after addition of lentivirus. Cells were collected 72 hours following siRNA transfections.

Immunofluorescence, IF-PNA FISH and subtelomeric FISH

For anti-Hop2 immunofluorescence, permeabilized coverslips were blocked with 10% goat serum for 30 minutes at 37°C, followed by incubation with primary antibody for 16h at 37°C. Coverslips were washed and incubated with appropriate secondary antibody for 20 minutes at 37°C, then mounted onto glass slides using Vectashield mounting medium with DAPI (Vector Labs).

edU fluorescence assay

16 hours after cells were transfected with mCherry-ER-DD-TRF1FokI, media was changed to contain 10 μ M (final) edU. Cells were pre-incubated for 2 hours then Shield1 and 4-OHT were added to the media to induce TRF1FokI for 2 hours. Cells were fixed and edU was labeled with Alexa488 using Click-iT chemistry (Invitrogen).

Pulsed field gel electrophoresis and in-gel hybridization

Genomic DNA was purified using the Masterpure DNA Purification Kit (Epicentre) per manufacturer's instructions. 15 μ g of purified DNA was digested using AluI and MboI, and resolved on a 1% PFGE agarose gel (Biorad) in 0.5X TBE buffer using the CHEF-DRII system (Biorad) at 6V/cm; initial switch time 5, final switch time 5 for 10-16h.

Following electrophoresis, the gel was dried at 50°C for 3h and processed for native or denaturing probe hybridization. For native hybridization, the dried gel was incubated with p32 end labeled (TTAGGG)₆ oligo probe at 42° for 16h in Church buffer, washed 4 times in 4X SSC and exposed onto a storage phosphor screen (GE Healthcare) and scanned using STORM 860 with ImageQuant (Molecular Dynamics). For denaturing hybridization, the gel was denatured in 0.5N NaOH/1.5M NaCl, neutralized and incubated with p32 end labeled (TTAGGG)₆ oligo probe as above.

Nuclease digestion of genomic DNA

For Bal31 digestion, purified genomic DNA (5ug) was incubated with Bal31 (2 units per reaction, TaKaRa/Clontech) in buffer provided by manufacturer for various timepoints at 30°C, followed by inactivation in 20mM EDTA at 65°C for 10 minutes. The Bal31 digested DNA was then purified by phenol-chloroform extraction and resolved by PFGE as above. For Exo1, purified genomic DNA (10ug) was incubated with Exo1 for 16h at 37°C, purified with phenol-chloroform extraction and resolved by PFGE.

C-circle Assay

Purified genomic DNA was digested using AluI and MboI (New England Biolabs). 15ng or 30ng of DNA was diluted to 10ul, then combined with 10ul of 0.2 mg/ml BSA, 0.1% Tween, 1mM each dNTP without dCTP, 1x ϕ 29 Buffer (NEB) and

7.5U ϕ 29 DNA polymerase (NEB). Samples were incubated for 8 hours at 30°C then the polymerase was inactivated for 20 minutes at 65°C. Samples were diluted with 2x SSC to 60ul, then dot-blotted onto Hybond N+ membrane (GE Healthcare). After UV crosslinking, the membrane was hybridized with p32 labeled (CCCTAA)₆ oligo at 37°C in Church buffer for 16h. Membrane was exposed onto a storage phosphor screen (GE Healthcare) and scanned using STORM 860 with ImageQuant (Molecular Dynamics).

Chromosome orientation FISH (CO-FISH)

Telomeric CO-FISH can be used to assess the level of postreplicative exchanges involving a telomere and another TTAGGG repeat sequence, and has been described in detail previously (Bailey et al., 2004; Londono-Vallejo et al., 2004). Briefly, cells were incubated with BrdU/BrdC (7.5 μ M, 2.5 μ M respectively) for 21h (less than one cell cycle). Mitotic cells were collected after treatment with 0.1 μ g/ml colcemid for 90 minutes. Subsequently, cells were incubated in 75 mM KCl and fixed on ice with fresh fixative (3:1 methanol / acetic acid). Fixed cells were dropped onto slides at 42°C, and allowed to dry o/n. The slides were treated with 0.5mg/ml RNaseA for 15 minutes at 37°C, then with 0.5mg/ml Hoechst 33258 for 15 minutes at RT. Slides were exposed to 365nm UV light for 30 minutes to introduce nicks in the BrdU/C incorporated replicated strands. The nicked strands were digested twice with 10U/ul ExonucleaseIII (Promega) in buffer supplied by manufacturer at RT for 10 minutes. Ethanol dried slides were stained with TelC-Cy3 and TelG-Alexa488 PNA probes (Panagene).

Live cell imaging

Cells were transfected with mCherry-ER-DD-TRF1-FokI 16 hours prior to induction with 4-OHT and Shield1 ligand for 60 minutes. Confocal images were acquired under temperature controlled conditions calibrated to 37°C, using a 100x 1.4 NA objective on an inverted fluorescence microscope (DM6000, Leica Microsystems) equipped with an automated XYZ stage (Ludl Electronic Products), a charge-coupled device camera (QuantEM 512SC, Photometrics), an X-LIGHT Confocal Imager (Crisel Electrooptical Systems), and a SPECTRA X Light Engine (Lumencor), controlled by Metamorph Software (MDS Analytical Technologies). Images were collected as z stacks at 0.6 μm intervals that covered the entire nucleus, at 2-minute intervals for a total of 60 minutes. Images were processed using ImageJ (NIH). Each z stack was projected onto a single z plane for each timepoint, and then the t stack was registered using StackReg plugin in ImageJ to normalize for cell movement. Tracking of individual foci was performed using the TrackMate plugin for ImageJ (Perry N, Tinevez JY and Schindelin J). The Mean Square Displacement (MSD) values were calculated using $MSD = \langle (x(t+\Delta t) - x(t))^2 \rangle$, where x is the position of the telomere and t is time in minutes. Resulting data were analyzed and visualized in MATLAB (MathWorks) using the class @msdanalyzer (written by JY Tinevez, Institute Pasteur). The error bars for each data point represent the weighted s.e.m. where weights are set to be the number of points averaged to generate the MSD value at the given delay.

The MSD trajectories were fitted to a single exponential diffusion model described by $MSD = \Gamma t^\alpha$ where Γ is a generalized coefficient, and α is a time dependence coefficient. The fitting was performed using least-squares fitting in GraphPad Prism.

Calculation of the time dependent diffusion coefficient was performed by calculating $D(t) = MSD/t = \Gamma t^{\alpha-1}$ (Saxton, 2007). For particles undergoing anomalous/subdiffusion, $D(t)$ decreases linearly with time with a slope of $\alpha-1$ when plotted on a log-log scale.

For analysis of clustering telomeres as in Figure 3G, H, telomere tracks were pre-selected for those that displayed clustering during the course of imaging. Telomeres that clustered during the final 2/3 of the movie were selected to ensure enough datapoints for movement preceding the association event. Then, the last 10 time points for each of these tracks were used for analysis (last 10 points prior to the joining event). For the analysis of incoming and recipient telomeres vs. post merge as in Figure 3I, clustering events that occurred during the middle 1/3 of the movie were analyzed.

Analysis of telomere foci size and clustering

For measurements of telomeric foci size, ImageJ (NIH) was used to apply a constant threshold to images and subsequent binarization. Foci sizes were measured as square pixels for each telomeric focus within a nucleus and the average size was calculated for each nucleus analyzed. For analysis of clustering following siRNA

transfection, a cluster was defined as a telomeric focus equal to or greater than four-fold the area as based on the radius, compared to the average size of undamaged telomeres.

Statistics

Unpaired *t* tests were used to generate two-tailed p values.

CHAPTER 3. Regulation of ALT telomere recombination by the ATR- Chk1 kinase pathway

I. Introduction

A network of signaling pathways ensure proper coordination of the complex sequence of molecular reactions that are required for completion of DNA repair. Double-strand breaks will activate ataxia-telangiectasia mutated (ATM) kinase. If the DSB is further resected to reveal single-stranded DNA onto which RPA rapidly binds, this structure recruits and activates ataxia-telangiectasia mutated and Rad3-related (ATR) kinase (Ball et al., 2005). Importantly, ATR is also activated during normal replication when ssDNA is exposed and ensures proper progression of the replication fork especially during periods of replication stress (Flynn and Zou, 2011). Downstream of ATM and ATR kinase activation, Chk2 and Chk1 kinases are phosphorylated respectively (Falck et al., 2001; Liu et al., 2000). Subsequent phosphorylation-mediated inhibition of Cdc25A/B/C phosphatases results in inhibition of cyclin-dependent kinases (CDKs), leading to cell cycle arrest. This temporary block allows sufficient time for completion of DNA repair.

The ATR-Chk1 pathway is critical for protection during replication stress both locally and globally. At the stalled replication fork, ATR stabilizes the structure of the fork and prevents collapse of the fork (Cobb et al., 2003; Lucca et al., 2004). In the absence of ATR, collapsed forks could degenerate into DSBs by structure-specific nucleases such as Mus81, posing a particular threat to cellular viability (Doe et al., 2002).

ATR also phosphorylates Chk1, which diffuses globally throughout the nucleus to suppress new origin firing (Shechter et al., 2004; Sorensen and Syljuasen, 2012). Inhibition of ATR or Chk1 results in deregulated origin firing and generation of DSBs globally from collapsed forks, leading to irreversible catastrophe and cell death (Buisson et al., 2015; Toledo et al., 2013).

It was recently shown that ALT activity is disrupted upon ATR inhibition and that ALT positive cells are selectively killed by ATR inhibition (Flynn et al., 2015). RPA coated ssDNA telomeres, characteristic of ALT cells, likely serves as a substrate to activate ATR. However, it is unclear how ATR would regulate ALT activity. One possibility is a direct effect of ATR-mediated phosphorylation on proteins mediating ALT recombination. Alternatively, ATR inhibition may exert its effects through disruption of replication at telomeres as well as the rest of the genome. In this section, I show that inhibition of ATR or Chk1 activities disrupt Rad51 and Hop2 localization to ALT telomeres, and that prevention of excessive replication origin firing and DSB generation partially alleviates this stress.

II. Inhibition of ATR and Chk1 activity disrupts HR factor localization at ALT telomeres

To test if ATR or Chk1 activity contributes to ALT telomere recombination by altering recruitment of HR factors, ALT cells were treated with small molecule inhibitors of ATR or Chk1 kinases. VE-821, which inhibits ATR with an IC₅₀ of 13nM in vitro,

and LY-2603618, which inhibits Chk1 with an IC50 of 7nM, strongly reduced Hop2 localization to telomeres in VA13 cells (Figure 15A, C). Hop2 localization was reduced to less than 50% by 4 hours of treatment, and continued to decline until 24 hours of treatment (Figure 15 B, D). CHIR-124, another potent Chk1 inhibitor with an IC50 of 0.3nM, reduced Hop2 colocalization with telomeres similarly to LY-2603618 in VA13 cells (Figure 15F). Reduction of Hop2 at telomeres by ATRi was also apparent in GM847, another ALT cell line (Figure 15 E). Knockdown of ATR recapitulated the loss of Hop2 in VA13 cells, while knockdown of ATM only marginally affected Hop2 and knockdown of RNF168 significantly increased Hop2 localization to telomeres (Figure 15G).

In order to test if localization of other HR factors is affected by ATR and Chk1 inhibition, RPA and Rad51 were visualized at ALT telomeres by immunofluorescence. Interestingly, RPA32 foci maintained colocalization with telomeres even after treatment with VE-821 in VA13 cells (Figure 16A, B). U2OS cells expressing TRF1-FokI also largely retained RPA32 foci after treatment with VE-821 or LY-2603618 (Figure 16E). On the other hand, inhibition of ATR and Chk1 significantly reduced Rad51 recruitment to telomeres similarly to Hop2 (Figure 16C, D, F). These results show that ATR or Chk1 inhibition, but not ATM or RNF168 inhibition, specifically perturb Rad51 and Hop2 localization to ALT telomeres while RPA recruitment is unaffected.

III. Inhibition of ATR and Chk1 results in genome-wide DNA fragmentation

Since ATR inhibition results in replication fork breakage and DSB generation (Toledo et al., 2013), we tested whether telomeres in ATR or Chk1-inhibited ALT cells could be fragmented. Indeed, VA13 cells treated for 24h with VE-821 or LY-2603618 revealed numerous nuclei with striking increase in fine telomere PNA signals suggestive of telomere DNA breakage (Figure 17A). The nature of the fine PNA signal is unlikely to be from generation of extrachromosomal C-circles, since their abundance is unchanged with ATRi or Chk1i (Figure 17B). In order to confirm that telomeric DNA is being fragmented, cells treated with VE-821 or CHIR-124 were embedded in agarose plugs and subjected to pulsed-field electrophoresis in the absence of liberation of DNA by enzymatic digestion (Saleh-Gohari et al., 2005). This method allows visualization of DNA fragments that would otherwise be trapped in or near the plug if they were still part of the intact chromosomal DNA. Treatment with VE-821 or CHIR-124 resulted in increases in telomere fragments that were most apparent at 24 hours (Figure 17C-E). To test if breakage was occurring exclusively at telomeres, fragmentation at non-telomeric locations was assessed using probes recognizing the Alu repeat sequence. This analysis revealed that ATRi- or Chk1i-induced breaks are not exclusive to telomeres (Figure 17C, D). In fact, breaks containing the Alu sequence increased more rapidly than those containing the telomeric sequence (Figure 17E).

Recent data suggests that generation of DSBs and single stranded DNA from ATRi and Chk1i occurs during S phase (Buisson et al., 2015; Toledo et al., 2013). To analyze the relationship between emergence of DNA breaks and cell cycle, SV40-transformed ALT cell line derived from primary human fibroblasts, LM216J^{ALT}, was

treated with VE-821 or CHIR-124 and analyzed by flow cytometry for γ H2Ax and propidium iodide (PI) signal (Figure 18A, B). With VE-821 treatment, the percentage of cells positive for γ H2Ax doubles by 8 hours and there is a three-fold increase by 24 hours. For CHIR-124, the percentage of γ H2Ax-positive cells increases more rapidly. By 4 hours, there is a four-fold increase and by 24 hours, there is a 10-fold increase in the percentage of cells that are γ H2Ax positive. For both inhibitors, the rise in γ H2Ax occurs mostly in S/G2 populations (Figure 18A, B).

To test whether this increase in γ H2Ax was specific for ALT cells, LM216T^{TEL} cells, which express telomerase and are ALT-negative, were analyzed also by flow cytometry after treatment with VE-821 and CHIR-124. The percentage of total γ H2Ax positive LM216T^{TEL} cells increased similarly to LM216J^{ALT} cells (Figure 18A, B). Interestingly, in LM216T^{TEL} cells, the increase in γ H2Ax occurred not only in S/G2 cells but also in G1 cells. This is unanticipated and the mechanism for generation of breaks in the G1 population requires further investigation. Regardless, it can be concluded that the phenotype of DNA fragmentation following ATR or Chk1 inhibition is not specific to the ALT status of cells.

IV. Limiting replication-dependent fork breakage partially rescues the loss of Rad51 and Hop2 from ALT telomeres

Previous studies have reported that DNA fragmentation following ATR or Chk1 inhibition can be suppressed by limiting new origin firing by administration of a CDK-

inhibitor roscovitine and by reducing processing of stalled replication forks by knockdown of Mus81 nuclease (Buisson et al., 2015; Toledo et al., 2013). Indeed, treatment of VA13 cells with roscovitine strikingly reduced ATRi and Chk1i-dependent DNA fragmentation assessed by southern blot (Figure 19A). The percentage of γ H2Ax positive cells also decreased 10-fold by treatment with roscovitine (Figure 19B). One possibility is that generation of DNA fragments could divert factors such as Hop2 or Rad51 away from telomeres in a dilution manner since DSBs are prevalent throughout the nucleus. If so, reduction of DSBs by roscovitine treatment or Mus81 knockdown should allow Hop2 and Rad51 to return to telomeres. In VA13 cells, treatment with roscovitine or Mus81 knockdown by siRNA transfection partially rescued Rad51 and Hop2 localization to telomeres (Figure 19C-F). While roscovitine almost completely prevented DSB generation by ATRi or Chk1i, the magnitude of rescue of Rad51 or Hop2 was only 30-50%. This strongly suggests that ATR and Chk1 inhibition works through additional mechanisms to suppress Rad51 or Hop2 localization to telomeres.

V. Abrogation of Hop2 expression by CRISPR/Cas9 disrupts ALT activity

In order to test the effect of complete Hop2 loss from ALT cells, we utilized the CRISPR/Cas9 system to stop the expression of Hop2 in VA13 cells. Several guide RNAs targeting exon 1 of Hop2 were each transfected into VA13 cells along with Cas9 expression, and resulting cell populations were analyzed by western blotting (Figure 20A). The guide RNAs demonstrated varying levels of efficiency in terms of reduction in Hop2 expression. Interestingly, the guide sequence sgHop2-b resulted in an absence of

any detectable Hop2 expression by western. This was confirmed by the complete absence of Hop2 immunofluorescence signal in VA13 cells (Figure 20B). Cells selected for sgHop2-b expression (VA13 sgHop2) were then analyzed for ALT activity. Compared to the parental VA13 cells, sgHop2 cells demonstrated a 50% reduction in number of telomere PNA signals colocalizing with PML (APBs) (Figure 20C, D). Furthermore, clustering was reduced in sgHop2 cells as assessed by average telomere PNA FISH foci size (Figure 20E). BrdU incorporation occurring outside of S phase was also reduced, along with the frequency of telomere exchanges assessed by CO-FISH assay (Figure 20F, G). The reduction of ~50% in ALT activity is similar to the effect observed by Hop2 knockdown using siRNA.

VI. Discussion

One of the unique characteristics of ALT cells that distinguish them from telomerase positive cells or non-stem somatic cells is the persistent localization of RPA at telomeres (O'Sullivan et al., 2014). This substrate is likely recognized by ATR; however, the events occurring downstream of ATR activation in ALT cells is unclear. Here, we show that HR factor localization is significantly reduced upon ATR or Chk1 inhibition. Hop2 and Rad51 were rapidly removed from telomeres within 4 hours of treatment with ATR or Chk1 inhibitors, while knockdown of ATM or RNF168 did not have the same effect. Interestingly, RPA localization did not decrease following ATRi or Chk1i, suggesting that the effect of ATR or Chk1 inhibition on Hop2 and Rad51 localization is downstream of RPA loading onto telomeres.

ATR and Chk1 kinases possess an overwhelming number of phosphorylation substrates that coordinately serve to protect the genome in situations such as replication stress and fork stalling/collapse. In the absence of the kinases, one of the most striking phenotypes is the generation of DNA DSBs resulting from unregulated origin firing and resultant fork collapse. In ALT cells, ATR and Chk1 inhibition results in fragmentation of telomeric DNA as shown by the appearance of numerous fine telomere PNA FISH signals and by the increase in mobile DNA fragments during electrophoresis. However, this fragmentation is not specific to telomeres and occurs throughout the genome, resulting in large increases in percentage of γ H2Ax positive cells. In agreement with previous reports, this breakage was reversed upon suppression of new origin firing with roscovitine or conversion of stalled forks into DSBs by Mus81. These findings strongly support a model in which the ATRi/Chk1i-induced fragments are generated during S and G2 phases of the cell cycle and are dependent on conversion of replication forks into DSBs.

We tested the hypothesis that the generation of DNA DSBs upon ATR or Chk1 inhibition contribute to the absence of Hop2 and Rad51 from ALT telomeres. However, while DSBs and γ H2Ax were almost completely reduced, Rad51 and Hop2 localization to telomeres were only partially rescued. Furthermore, reduction of Rad51 and Hop2 occur rapidly following addition of ATR or Chk1i (Figure 15B, D) whereas fragmentation is most apparent at 8-24hours of treatment (Figure 17C, D). These findings suggest that additional mechanisms, such as reduction of direct phosphorylation of Rad51 and/or Hop2, could contribute to their loss from telomeres upon ATRi or Chk1i.

Lastly, additional experiments are needed to investigate how ATR and Chk1 potentially function uniquely in ALT cells compared to non-ALT cells. When comparing ALT-positive LM216J cells to ALT-negative but telomerase positive LM216T cells, the levels of induction of γ H2Ax were similar between the two cell lines. One possibility is that with limiting amounts of HR proteins in the nucleus, the generation of DSBs would dilutionally draw these factors away from ALT telomeres, causing dysfunction. Whether ATR or Chk1 inhibition would affect ALT telomeres uniquely in this way remains to be tested.

VII. Experimental Procedures

CRISPR/Cas9 Cell line generation

The following primers were used as guide RNA sequences.

sgHop2-a: GCCGGACGTTGTAGTTGCTCG

sgHop2-b: GCGGGAAAGGCGATGAGTAA

sgHop2-c: GCGGGAGGTAACGGCGCCGT

sgHop2-d: GAGTAGATTCACCCGTTGTC

sgHop2-e: GACCCATGAGAGCCCGACAAC

To generate the cell lines, cells were first transduced with and selected for blasticidin resistance using lentivirus generated from lentiCas9-Blast plasmid (Sanjana et

al., 2014). Cells were then transduced with and selected for puromycin resistance using lentivirus generated from lentiGuide-Puro plasmids containing the guide RNA sequences targeting Hop2. Expression of Hop2 was assayed by Western blot 7 days after guide RNA transduction.

Chemical reagents

VE-821 (Selleck Chemicals) was used at a final concentration of 5 μ M. CHIR-124 (Selleck Chemicals) was used at a final concentration of 100 μ M. LY-2603618 (Selleck Chemicals) was used at a final concentration of 1 μ M. Roscovitine (Sigma) was used at a final concentration of 10 μ M.

DNA Fragmentation Assay

1 million cells were collected by trypsinization and embedded in 1% low melting point agarose plugs. Plugs were digested overnight in proteinase K digestion buffer (100mM EDTA pH 8.0, 0.2% sodium deoxycholate, 1% sodium lauryl sarcosine, 1mg/ml proteinase K) at 50°C. After washing in TE, DNA in digested plugs was resolved on a 1% PFGE agarose gel (Biorad) in 0.5X TBE buffer using the CHEF-DR11 system (Biorad) at 6V/cm; initial switch time 5, final switch time 5 for 16h. Following electrophoresis, the gel was dried at 50°C and processed for denaturing probe hybridization. The dried gel was denatured in 0.5N NaOH/1.5M NaCl, neutralized and incubated with p32 end

labeled (TTAGGG)₆ oligo probe overnight. The washed gel was exposed onto a storage phosphor screen (GE Healthcare) and scanned using STORM 860 with ImageQuant (Molecular Dynamics).

Flow cytometry

Cells were collected by trypsinization, washed in ice cold PBS and fixed in 70% ethanol. Permeabilized cells were stained with FITC-conjugated anti- γ H2Ax antibody (Millipore) and with propidium iodide. Cells were analyzed on BD FACSCALIBUR and data was analyzed using FlowJo software.

Chapter 4. Conclusions and Future Directions

The scope of the present thesis was to investigate the mechanisms of telomere recombination in alternative lengthening of telomeres. Understanding the mechanisms driving ALT is of important therapeutic significance since all cancers rely on one of two telomere maintenance mechanisms. While numerous therapeutic approaches target telomerase in an effort to treat ~85% of cancers that overexpress the enzyme, there are no available treatments for ALT-utilizing cancers, partly due to lack of a mechanistic understanding of ALT recombination. Major gaps in knowledge exist in terms of the initiating events leading to ALT, the nature of the substrates for recombination, the choice of recombination pathways, the composition of the recombination machinery and the mechanism for DNA synthesis during repair. The present thesis contributes to a model for ALT recombination that initiates from a DSB response-driven HR reaction. However, additional studies are required to further probe the linearity of this model by testing for other parallel recombination mechanisms that may coexist in ALT, and to understand how the actual DNA synthesis and elongation occurs to ensure survival of ALT cancers.

Generation of the TRF1-FokI system allowed coordinated induction of ALT activity and thus enabled a direct view of the initiating events during ALT telomere recombination. TRF1-FokI expression increased ALT activity, measured by levels of APB formation, C-circle generation, telomere heterogeneity and new DNA synthesis. Importantly, one of the most striking phenotypes of TRF1-FokI expression was a rapid induction of large clusters of telomeres that are found in varying sizes and numbers in

different ALT cell lines. Telomere foci sizes in U2OS cells are smaller than other cell lines at baseline, and this allowed us to visualize the formation of large telomere clusters.

Visualization of telomeres in live cells by expression of mCherry-tagged TRF1-FokI revealed rapid telomeric clustering events that occurred within 1-2 hours of TRF1-FokI induction by Shield1 and 4-OHT. Similar clustering events were observed much more rarely in TRF1-FokI D450A mutant expressing cells in which no DNA cleavage occurs. Telomeres traversed between 1-5 μ m in nuclear distance to merge with a recipient telomere. Instead of moving randomly prior to collision with a second telomere, telomere foci moved directionally toward the recipient telomere, suggesting that an active process could be enforcing the merger of two foci.

We had noted that the chromatin state at ALT telomeres favors accumulation of HR factors instead of NHEJ. RPA normally colocalizes with ALT telomeres, which also accumulate recombination-promoting proteins such as BRCA1 while NHEJ-promoting 53BP1 remains at the periphery of telomere foci. Furthermore, telomere overhangs that are substrates for initiation of HR are prominent in ALT cells and are increased with TRF1-FokI. Thus, we tested whether Rad51, a recombinase that replaces RPA on ssDNA overhangs and is critical for homology search and D-loop formation, is required for ALT telomere movement. Clustering events and telomere movement were reduced upon knockdown of Rad51 by siRNA. Strikingly, GFP-Rad51 filaments could be directly visualized between merging telomeres, suggesting that Rad51-ssDNA nucleoprotein filament could directly bridge two recombining telomeres in order to facilitate their juxtaposition and synapsis.

The fact that ALT telomeres traverse several microns within the nucleus to merge with another telomere suggests that these recombination events are occurring between non-sister telomeres. This is a unique situation since the vast majority of HR reactions in somatic cells occur between homologous sequences on sister chromatids. On the other hand, a situation in which interchromosomal recombination preferentially occurs is during meiotic recombination. Crossover recombination occurs upon programmed DSB generation and juxtaposition of homologous chromosomes that are microns away in the nucleus. Interestingly, meiotic recombination requires a critical factor called Homologous-Pairing 2 (Hop2), which functions together with Mnd1 and the meiotic recombinase DMC1 to complete chromosome pairing (Leu et al., 1998; Pezza et al., 2007). Hop2 and Mnd1 were broadly expressed in all cancer cell lines tested, but its expression was limited in mortal fibroblast cell lines. Importantly, knockdown of Hop2 and Mnd1 reduced ALT telomere clustering and movement following TRF1-FokI expression. Furthermore, Knockdown of these proteins resulted in disruption of ALT activity by reducing APB formation and telomere exchanges in ALT cells even in the absence of TRF1-FokI.

These data show that ALT telomere recombination is intimately linked to the homologous recombination machinery and that a DSB response initiates a homology search requiring Rad51 and Hop2-Mnd1. A model for ALT could be proposed based on these findings: DSB responses at ALT telomeres triggers recruitment of HR factors that carry out a search for a homologous substrate, followed by synapsis, D-loop formation and DNA synthesis to complete the repair process. Questions remain as to how the HR

factor recruitment process is regulated, and how DNA synthesis proceeds following D-loop formation.

RPA-coated single stranded DNA is a substrate readily recognized by ATR kinase, which signals downstream to a number of different substrates such as Chk1. It is reasonable to hypothesize that RPA-coated single stranded telomeres, which are abundant in ALT cells, could activate ATR in order to trigger the recombination pathway. During normal recombination, RPA-coated single stranded DNA that becomes exposed recruits ATR to initiate a HR-dependent repair pathway that restores the replication fork. A similar process could take place during periods of replication stress at ALT telomeres occurring in the absence of ATRX (Clynes et al., 2015).

Inhibition of ATR or Chk1 with small molecule inhibitors resulted in a striking reduction of Rad51 and Hop2 localization to ALT telomeres within 4 hours of treatment. On the other hand, recruitment of RPA to telomeres did not decrease significantly upon ATRi or Chk1i, which is consistent with the expectation that inhibition of ATR would not affect the nature of the substrate that it recognizes. We hypothesized that the reduction in Rad51 and Hop2 could be directly due to the loss of their recruitment by ATR and Chk1, or indirectly due to the effect of ATRi and Chk1i on ALT cells. Since a prominent effect of ATRi and Chk1i is fragmentation of the genome from collapsed replication forks, we asked whether this phenomenon contributes to the loss of Rad51 and Hop2 from ALT telomeres by creating a catastrophic number of DSBs elsewhere in the genome that deplete the available pool of HR factors.

ATRi and Chk1i caused significant fragmentation of ALT telomeres, as evidenced by increased signal upon electrophoresis of free DNA fragments. The DSB generation was not specific to telomeres, but instead was global since breaks in Alu sequences, interspersed throughout the genome, were more prominent than telomeric breaks. These breaks could readily be detected using γ H2Ax staining of treated cells. As reported previously, the DSB generation from ATRi or Chk1i could be limited using roscovitine, a CDK inhibitor, or siMus81. We then analyzed whether elimination of DSBs during ATRi or Chk1i could rescue Rad51 and Hop2 loss from telomeres. Upon treatment with roscovitine or knockdown of Mus81, Rad51 and Hop2 localization was partially rescued even though roscovitine almost completely limited DSB and γ H2Ax generation. These results indicate that while genome-wide breaks following ATRi and Chk1i is a prominent feature that leads to cell death in treated cells, they do not wholly account for the loss of Rad51 and Hop2 from ALT telomeres. Further experiments are needed in order to understand potential mechanisms of ATR and Chk1-mediated recruitment of HR factors in ALT.

In sum, these data are consistent with a DSB-initiated HR-driven mechanism for ALT telomere recombination. However, several aspects of the model still remain unclear. How does the terminal process of DNA synthesis occur and which DNA polymerases are critical? Are there alternative or co-existing pathways for recombination in ALT?

A prediction from the proposed model is that ALT recombination events should culminate in synthesis of new DNA. In mammalian cells, there are 15 characterized DNA polymerases that could fulfill this role. A minority of these polymerases carries out

normal replication, while the majority performs various forms of DNA repair. Although direct evidence of DNA synthesis by these polymerases during repair has been lacking due to a lack of an appropriate mammalian system in which to study DNA synthesis, the polymerases that have been implicated in HR or NHEJ include Pol β , Pol ζ , Pol η , Pol θ , Pol λ and μ . Interestingly, Pol β was required for synapsis during meiosis, functioning at an early step in the processing of meiotic DSBs (Kidane et al., 2010). Pol η deficiency results in reduced gene conversion events that occur as a result of HR in chicken DT40 cells. Additionally, Pol η can perform repair synthesis *in vitro* to extend the end of the 3' overhang serving as a primer, resulting in second-end capture by Rad52, which is a critical step in HR repair reactions involving homology on both ends of the broken strand (McIlwraith and West, 2008).

For ALT telomere synthesis, the putative substrates undergoing recombination suggest a similar but distinct type of reaction known as break-induced replication (BIR) may occur. While a DSB within the body of the chromosome contains two broken ends that need to be repaired, a break at a telomere is a one-ended starting substrate. BIR has been most extensively studied in eukaryotes in the budding yeast *Saccharomyces cerevisiae*. During BIR, the initial steps of 3' ssDNA overhang generation and invasion into a region of homology seem to be shared with gene conversion events that occur with homology on both ends of the break. However, upon formation of the D-loop, conversion to a replication fork-like structure occurs involving leading- and lagging-strand synthesis. In yeast, the requirements for replication at this stage are distinct from those of normal S-phase replication where Pol ϵ performs leading strand copying while Pol δ copies the

lagging strand. Pol32, a component of the Pol δ complex, along with Pol α -Primase complex is required for yeast BIR while Pol ϵ is dispensable for the initial steps of synthesis (Lydeard et al., 2007). The mammalian homolog of Pol32 is PolD3, which was recently implicated in allowing survival of cells undergoing replication stress upon cyclin E overexpression by a BIR-like mechanism (Costantino et al., 2014). These data suggest that the mammalian Pol α , δ and ϵ complexes are prime candidates for interrogation in ALT telomere synthesis which potentially proceeds by BIR as it does in yeast telomerase-null survivors (McEachern and Haber, 2006). We have preliminary data using TRF1-FokI as a system to probe for newly synthesized DNA at the telomeres. These assays should prove useful for understanding the requirements of mammalian DNA polymerases for ALT telomere recombination and synthesis.

A second interesting question that arises from comparison to ALT in yeast is whether different mechanisms of ALT recombination could exist. In *S. cerevisiae*, two pathways allow “survivors” to form in the absence of telomerase, both of which require Rad52 but only one of which requires Rad51 (Louis et al., 1994; Lundblad and Blackburn, 1993; Teng and Zakian, 1999). The first pathway (Type I) is characteristic for amplification of subtelomeric Y' elements along with telomeric repeats, and is dependent on Rad51 along with Rad52 and Rad54 (Le et al., 1999; Teng and Zakian, 1999). The second pathway (Type II) is notable for long and heterogeneous amplifications involving only telomeric repeats, and does not require Rad51 but relies on Rad52, the MRX complex and Rad59 (Lundblad and Blackburn, 1993).

We have observed that knockdown of Rad51 and Hop2 proteins resulted in ALT activity decreases of about 50% across the different assays that were employed including APB formation and telomere exchanges. These observations leave open the possibility that complementary mechanisms could replace the functions of Rad51 in mammalian cells. This idea is supported by the observation that yeast BIR can also proceed in Rad51-dependent and -independent manners (Ira and Haber, 2002; Malkova et al., 2001; Signon et al., 2001). A prediction of this model would be that concurrent inhibition of complementary pathways on which human ALT cells depend would be more effective in reducing ALT activity and inducing cell death. The initial candidates to test in this context are human Rad52, the Mre11-Rad50-Nbs1 (MRN) complex, BLM and WRN helicases and ATR (Cohen and Sinclair, 2001; Huang et al., 2001; Johnson et al., 2001; Signon et al., 2001; Tsai et al., 2002).

Understanding the mechanisms in play during ALT telomere recombination has become an exciting field that provides a system for interrogating poorly characterized repair pathways in mammalian cells and offers an opportunity to develop rational strategies for targeting ALT-positive tumors. I hope that the work presented in this thesis will be useful for subsequent studies of ALT telomeres and homologous recombination.

Figures

Figure 1

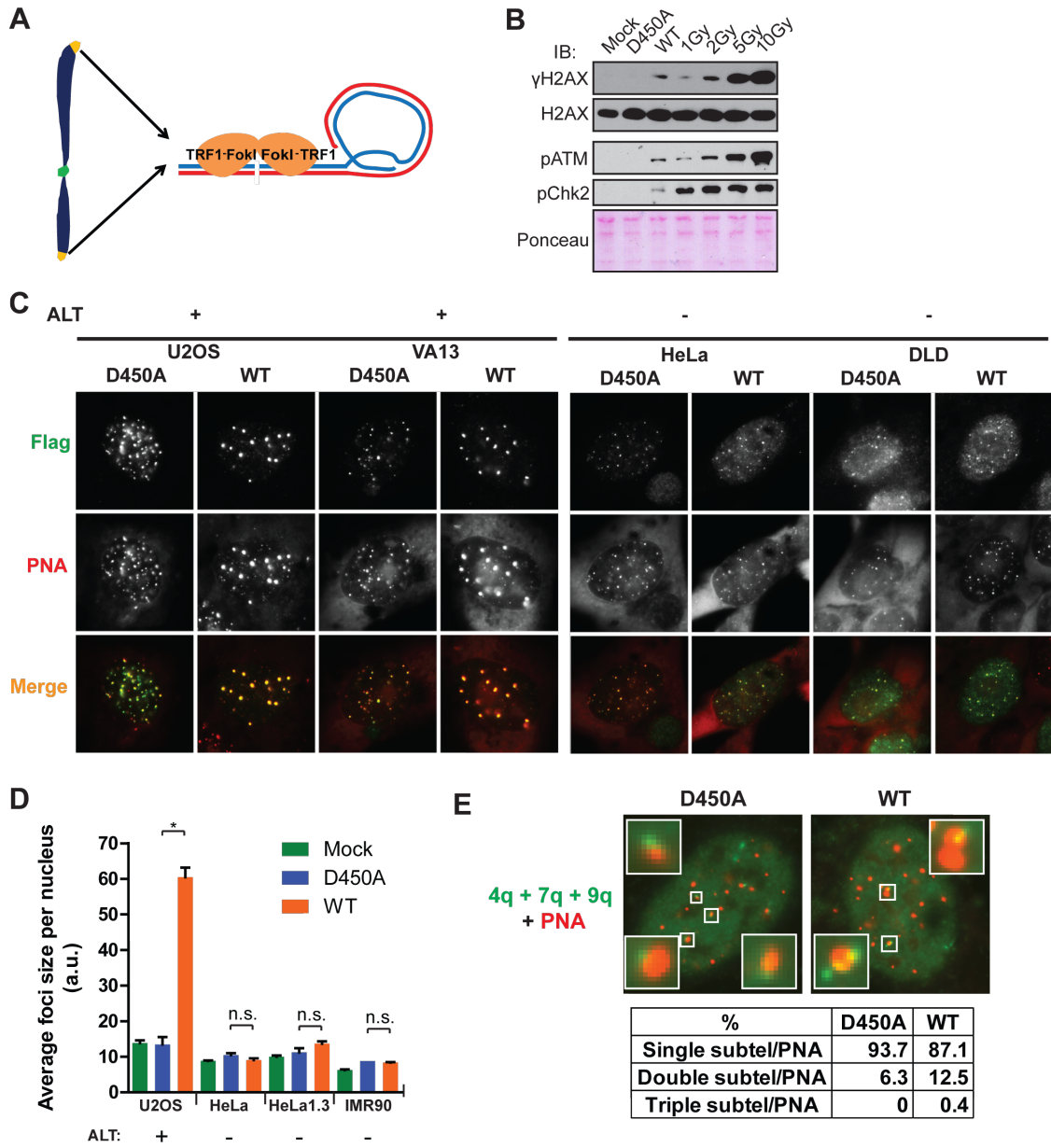


Figure 1. TRF1-FokI DSBs Promote Telomeric Clustering in ALT Cells

(A) Schematic of telomere-specific DSB induction by the TRF1-FokI fusion protein.

(B) Comparison of DSB responses in U2OS cells between TRF1-FokI expression and escalating doses of IR. Immunoblot (IB) was performed at 30 minutes following irradiation. Mock indicates mock viral transduction; D450A and WT indicate nuclease inactive and wild type TRF1-FokI, respectively.

(C) Representative immuno-FISH images of TRF1-FokI (Flag) WT or D450A colocalized with telomeres (PNA) in ALT positive and negative cells.

(D) Average telomere foci size per nucleus after TRF1-FokI expression was calculated using ImageJ. Mean \pm standard error of the mean (s.e.m.) for >50 cells in $n = 3$. * $p < 0.05$, n.s. $p > 0.05$.

(E) FISH was performed in cells expressing TRF1-FokI WT or D450A using a combination of chromosome-specific subtelomeric (subtel) probes and PNA. Percentages of colocalized subtel-PNA foci that contained one, two or three subtelomeric signals were quantified from >100 cells in $n = 2$.

Figure 2

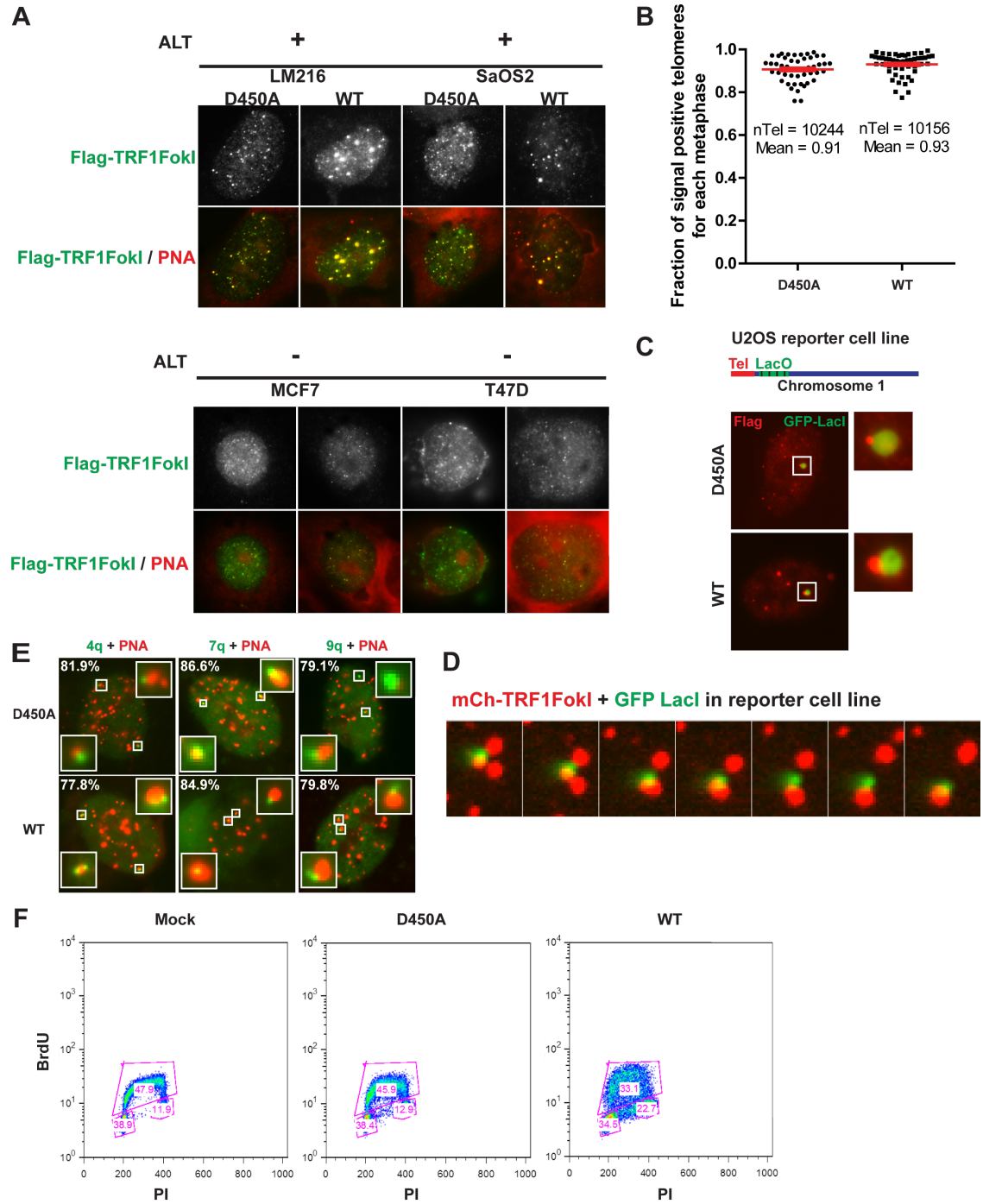


Figure 2. TRF1-FokI Induced Clustering Occurs Specifically in ALT Cells

(A) Cells that were mock treated or transduced with TRF1-FokI WT or D450A virus were incubated with BrdU for 1 hour then analyzed by flow cytometry.

(B) Representative immunofluorescence images for two additional ALT and telomerase positive cell lines after expression of TRF1-FokI WT or nuclease inactive D450A mutant.

(C) Fraction of PNA signal positive telomeres per total ends for each metaphase was quantified after TRF1-FokI expression. Mean of >40 metaphases were calculated from 2 independent experiments.

(D) GFP-LacI and TRF1-FokI were co-expressed in U2OS reporter cell line with LacO repeat sites integrated into a subtelomeric genomic locus at 1p36.

(E) FISH was performed in cells expressing TRF1-FokI WT or D450A, using the indicated chromosome-specific subtelomeric probes and PNA. Percentages indicate percentage of subtelomeric signals that are adjacent to a telomeric signal, quantified from >100 cells in two independent experiments.

Figure 3

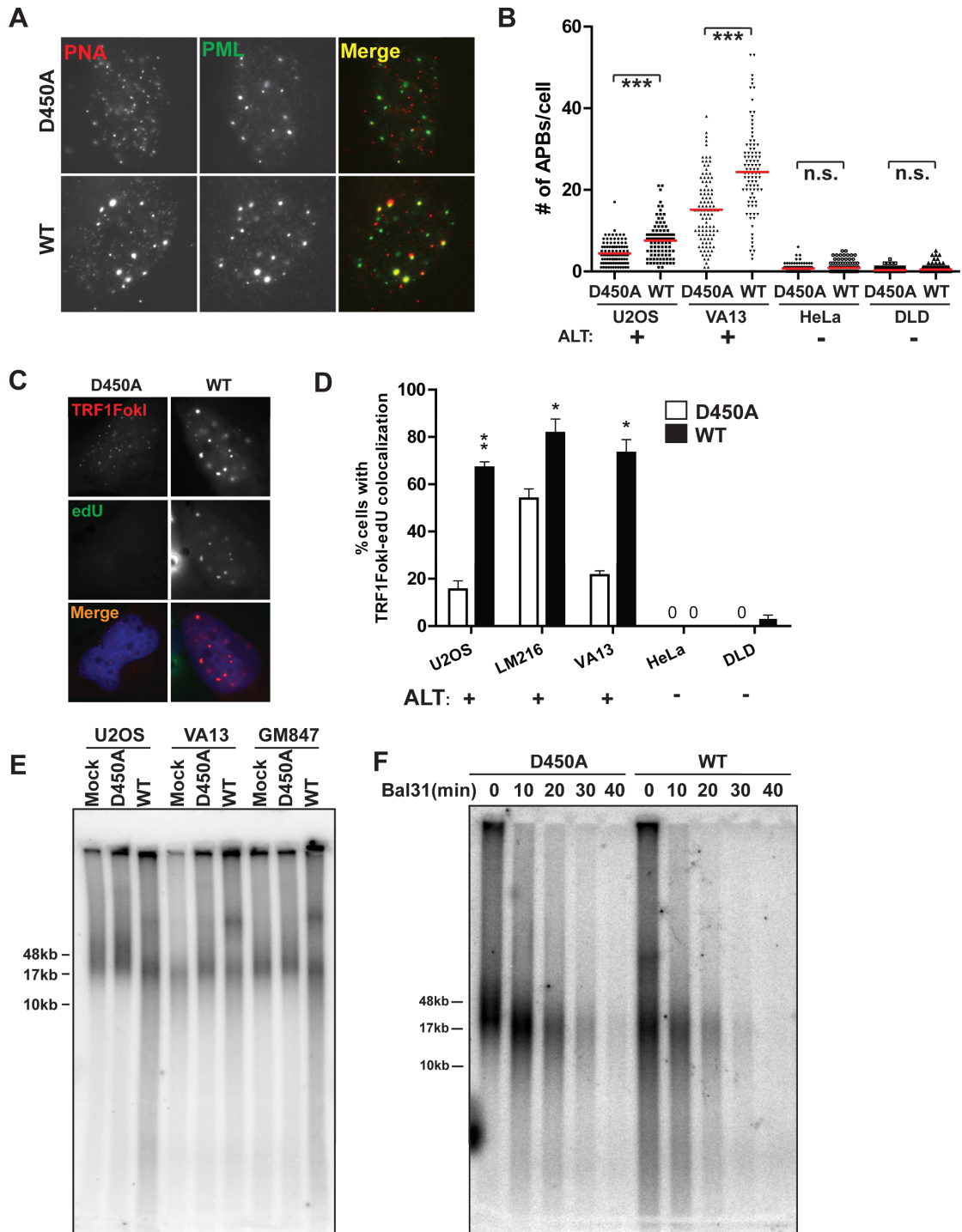


Figure 3. TRF1-FokI DSBs Promote ALT Activity

(A) Representative PNA/anti-PML immuno-FISH images of cells expressing TRF1-FokI WT or nuclease inactive D450A mutant.

(B) Number of PML-PNA colocalizations (APBs) per nucleus was quantified in cells expressing TRF1-FokI WT or D450A. Mean of >100 cells from three replicate experiments. *** $p < 0.005$, n.s. $p > 0.05$.

(C) Representative images of edU positive TRF1-FokI foci in VA13 cells.

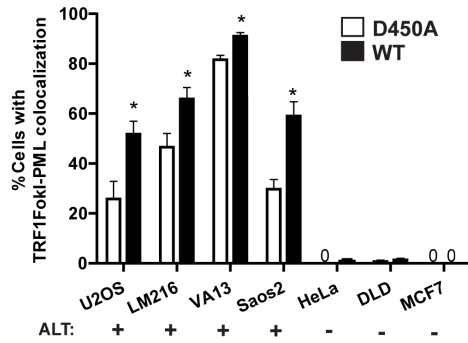
(D) Fraction of nuclei with ≥ 3 TRF1-FokI telomere foci colocalizing with edU foci in non-S-phase cells was quantified after expression of TRF1-FokI as indicated. Mean \pm s.e.m., >50 cells in $n = 3$. * $p < 0.05$.

(E) Digested genomic DNA from cells expressing TRF1-FokI was resolved by pulsed-field gel electrophoresis (PFGE) and probed for total telomeric DNA.

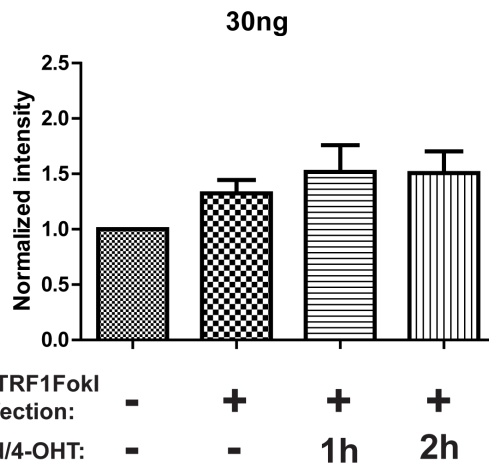
(F) Digested genomic DNA from U2OS cells expressing TRF1-FokI WT or D450A were treated with Bal31 nuclease for the indicated durations, resolved by PFGE and probed for total telomeric DNA.

Figure 4

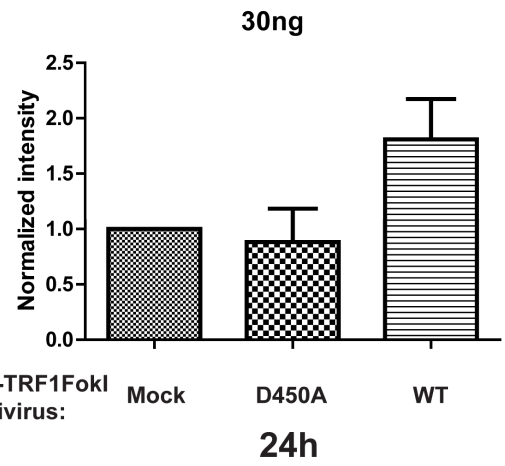
A



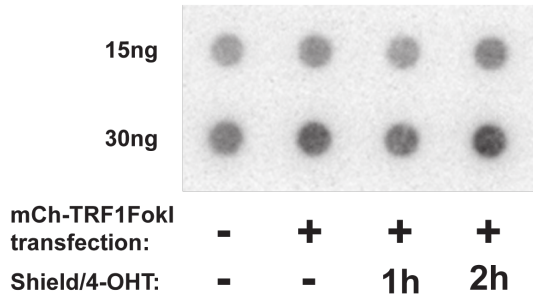
B



D



C



E

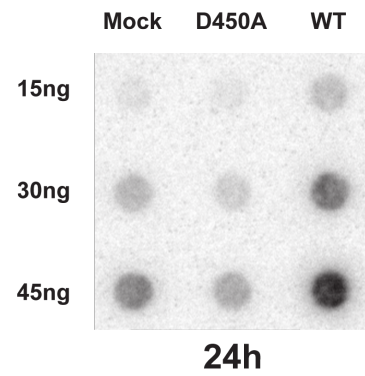


Figure 4. TRF1-FokI DSBs Promote ALT Activity

(A) The percentage of cells with ≥ 3 telomere foci colocalizing with PML was quantified in the indicated cell lines following TRF1-FokI expression (Mean \pm s.e.m., >50 cells in $n = 3$. * $p < 0.05$).

(B-C) U2OS cells were transfected with mCherry-TRF1-FokI and induced with Shield1 and 4-OHT for the indicated durations, and c-circle assay was performed using the indicated amounts of genomic DNA. Mean \pm s.e.m., $n=4$.

(D-E) U2OS cells were transduced with mock, TRF1-FokI D450A or WT virus for 24 hours and c-circle assay was performed using the indicated amounts of genomic DNA. Mean \pm s.e.m., $n=2$.

Figure 5

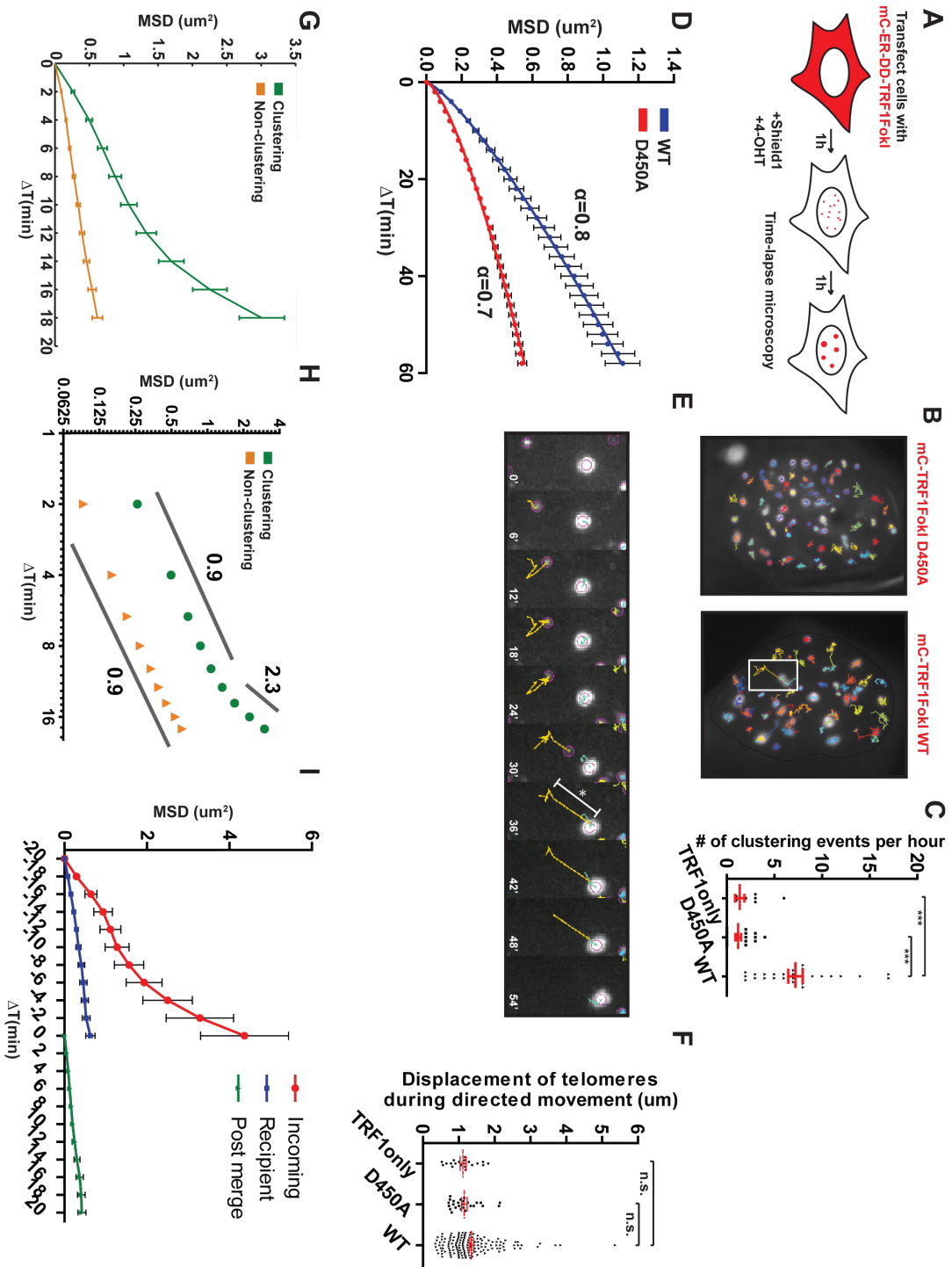


Figure 5. ALT Telomere DSBs Rapidly Associate by Long Range, Directional Movement

(A) Schematic of time-lapse imaging of telomeres in cells expressing TRF1-FokI. mC, mCherry; ER, modified estrogen receptor; DD, destabilization domain.

(B) Representative 1-hour traces of mCherryTRF1-FokI D450A or WT foci in U2OS nuclei. White box indicates region shown in (E).

(C) Quantification of telomere-telomere clustering where merged foci remain unseparated in 3 or more frames. In red, mean \pm s.e.m. Each datapoint represents tracked nuclei from two independent experiments. *** $p < 0.0005$. TRF1only represents mCherryTRF1 protein without C-terminal FokI.

(D) Mean squared displacement (MSD) analysis of telomere movement in U2OS cells expressing mCherryTRF1-FokI D450A or WT. Δt , time interval. Error bars, weighted s.e.m. and $n = >700$ tracks in two independent experiments. Fit was determined by a diffusion model, $MSD = \Gamma t^\alpha$, where α is the time dependence coefficient. $\alpha_{WT} = 0.8$ and $\alpha_{D450A} = 0.7$.

(E) Expanded images of a tracing from (B) highlighting diffusive movement followed by directed movement toward another telomere. * and bar denotes displacement measured in

(F). Yellow lines indicate the path traveled by the particle during the previous 10 frames.

(F) Quantification of telomere displacement during directed movement (mean \pm s.e.m of tracks from 2 independent experiments; n.s. $p > 0.05$). Directed phase was defined by

consecutive motion toward the recipient telomere over 3 or more frames until the merge event.

(G) MSD analysis of clustering telomeres in U2OS cells expressing TRF1-FokI WT (see text). $\Delta T=18$ represents the point of merge into a recipient telomere. $n = 157$ tracks from 2 independent experiments. Error bars, weighted s.e.m.

(H) Data from (G) is displayed on a log-log plot. Time dependence coefficient, α , for two phases of movement is indicated.

(I) MSD analysis of mobility before and after a merge event. $\Delta t=0$ represents the point of merge. Error bars, weighted s.e.m. and $n = 46$ tracks from two independent experiments.

Figure 6

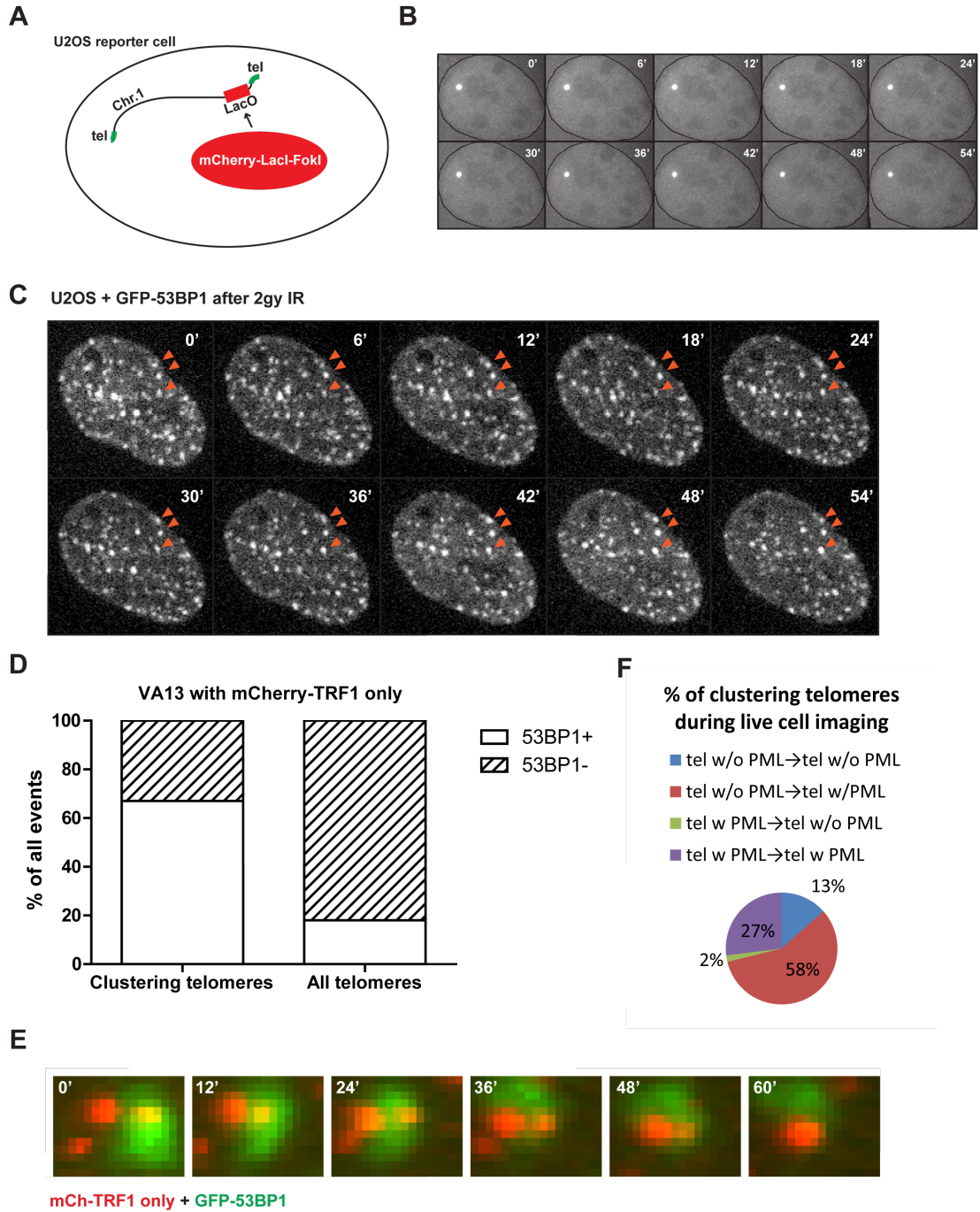


Figure 6. Damage-dependent Chromatin Movement in ALT is Telomere Specific

(A) Schematic of U2OS reporter cell line containing integrated LacO transgene proximal to the chromosome 1p telomere.

(B) Montage of live-cell images captured after induction of mCherry-LacI-FokI DSBs in the reporter cell line.

(C) Montage of live cell images in a representative U2OS cell expressing GFP-53BP1. Cells were treated with 2Gy IR and visualized after one hour. Arrowheads follow three GFP-53BP1 spots over the course of the experiment.

(D) mCherry-TRF1-FokI and GFP LacI were co-expressed in the U2OS reporter cell line and visualized with live cell imaging.

(E) Time-dependent diffusion coefficient $D(t) = MSD/\Delta t$ is plotted on a log-log scale for telomeres in cells expressing TRF1-FokI WT or D450A.

(F) Telomere clustering events in U2OS cells co-expressing mCherry-TRF1-FokI and GFP-PML were analyzed with respect to an associated GFP-PML signal.

(G) Live cell images of VA13 cells co-expressing mCherry-TRF1 only and GFP-53BP1 were analyzed for telomeres with or without colocalized 53BP1 signal.

(H) Montage of a representative clustering event in experiment in (G).

Figure 7

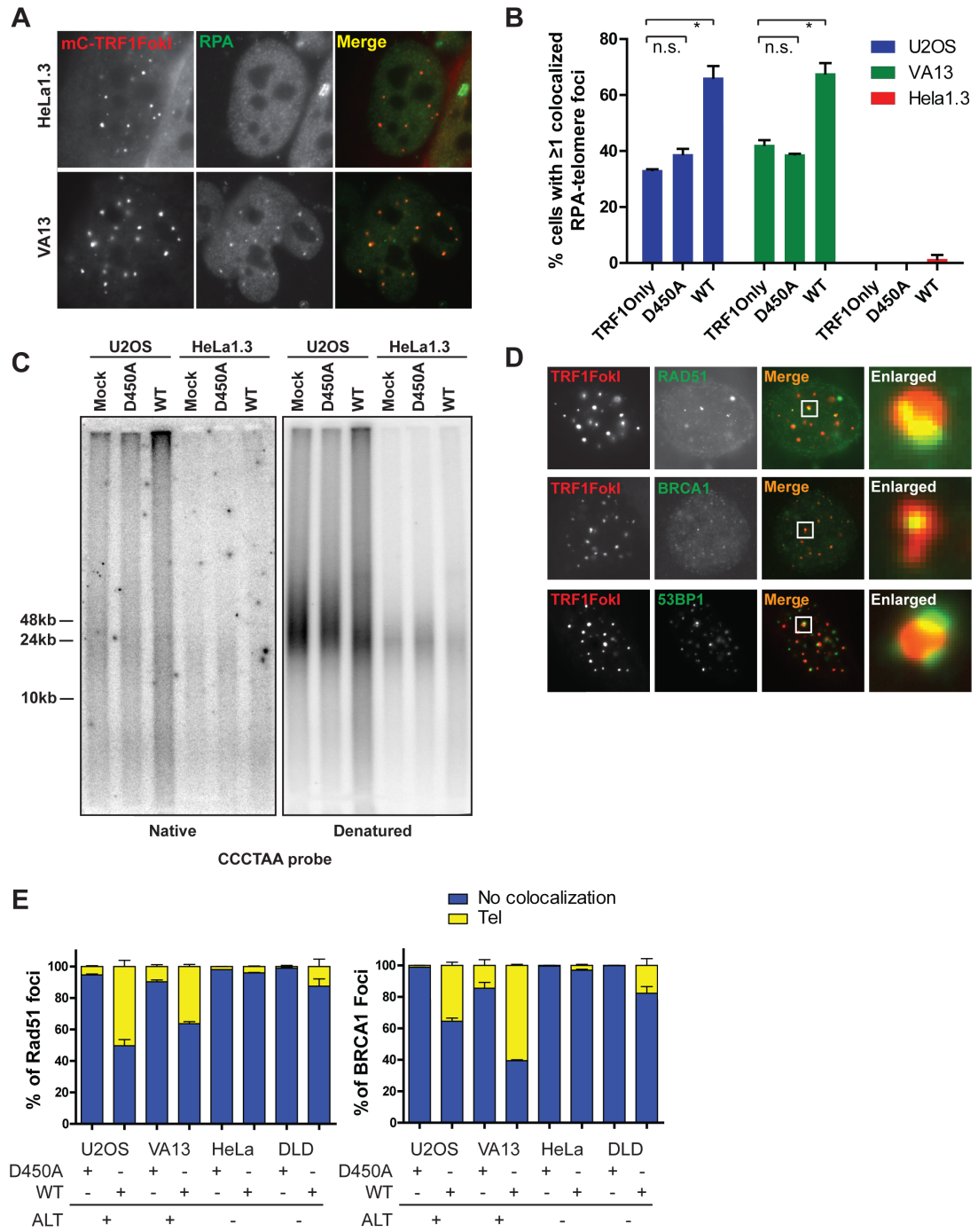


Figure 7. Homologous Recombination Predominates at ALT Telomere DSBs

(A) Representative immunofluorescence images of RPA2 and mCherry-TRF1-FokI WT in HeLa1.3 and VA13 cells.

(B) Quantification of RPA-telomere colocalization in ALT cell lines (U2OS and VA13) and a telomerase positive cell line (HeLa1.3).

(C) Telomeric DNA from U2OS and HeLa1.3 cells expressing TRF1-FokI D450A or WT was resolved by PFGE, and probed with p32 labeled oligos hybridizing to the G-rich single-stranded telomeres under native conditions. The gel was denatured and probed again for total telomeric signal.

(D) Representative immunofluorescence images of Rad51, BRCA1 and 53BP1 and mCherryTRF1-FokI WT and D450A positive telomeres in U2OS cells.

(E) Colocalization of Rad51 and BRCA1 to mCherryTRF1-FokI WT and D450A positive telomeres in ALT positive and negative cells. Tel, direct overlying colocalization to telomeres; Mean + s.e.m., n=2.

Figure 8

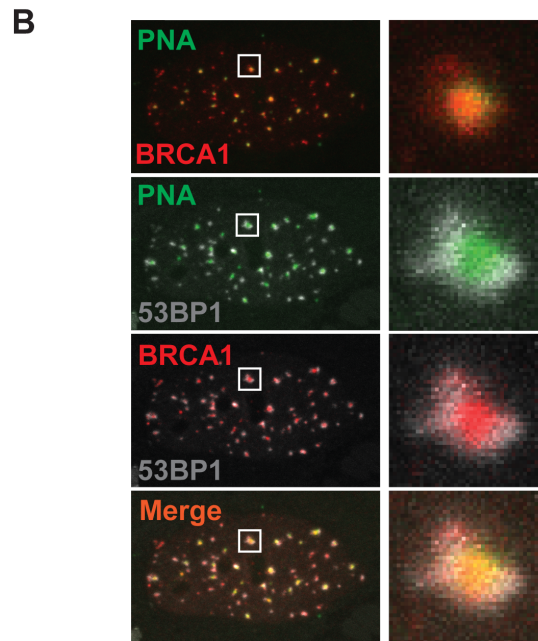
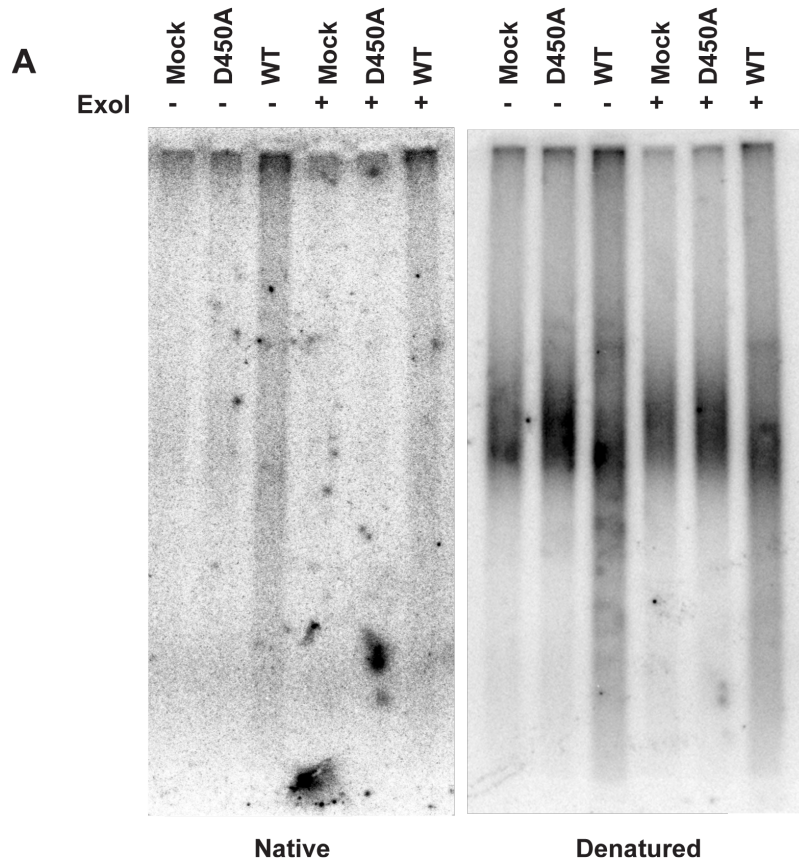


Figure 8. Increased Single-stranded Telomeric Signal is Largely from Telomeric Overhangs

(A) Digested genomic DNA from U2OS cells expressing TRF1FokI D450A or WT were treated with Exonuclease I prior to resolution by pulsed-field gel electrophoresis and hybridization under native and denatured conditions.

(B) Representative triple stained confocal microscopic images of native telomeres in ALT nuclei that accumulate 53BP1 and BRCA1.

Figure 9

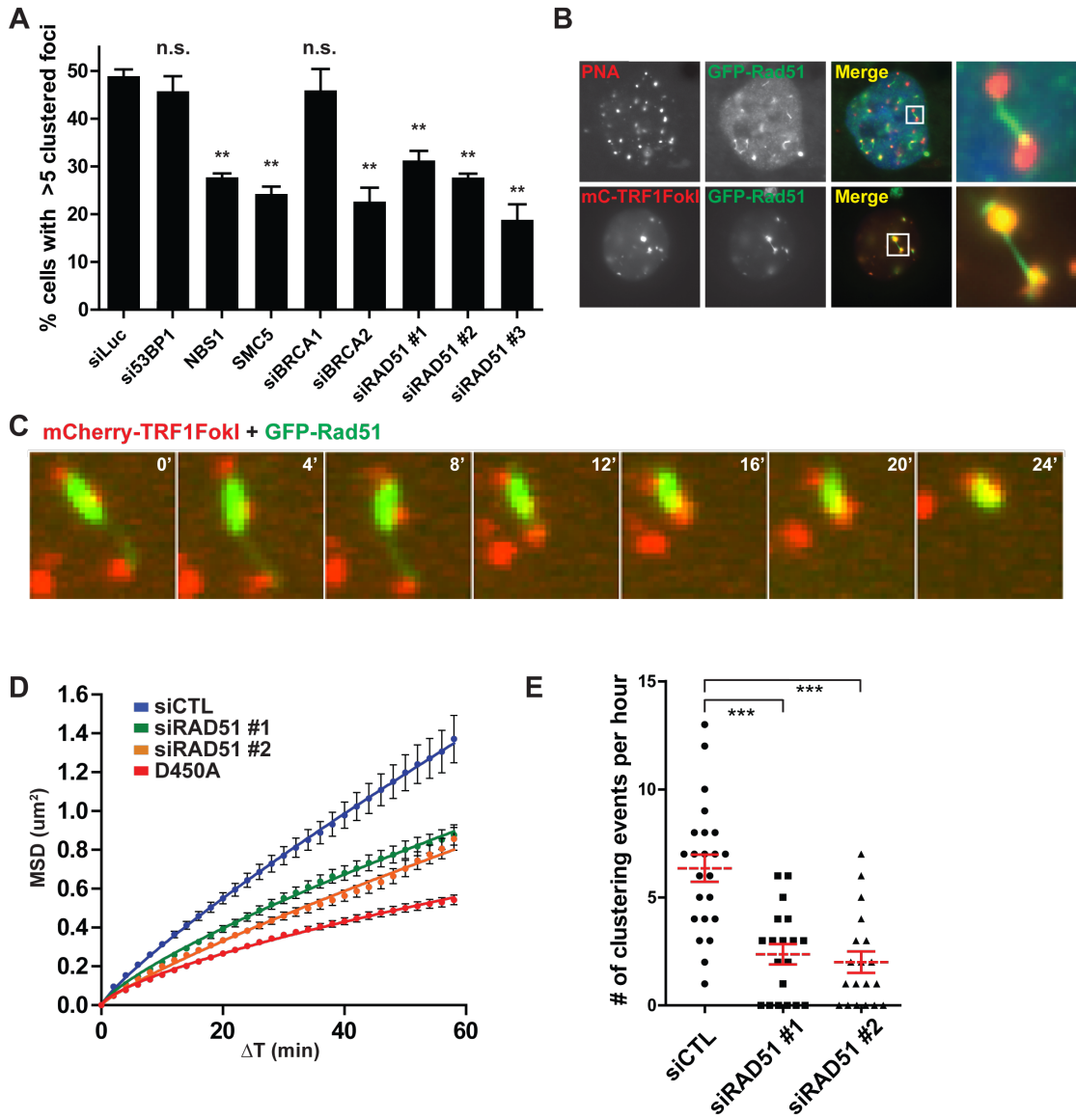


Figure 9. Rad51 Promotes Diffusive and Directed ALT Telomere Movement

(A) Quantification of TRF1-FokI induced telomere clustering at 72 hours following transfection of siRNA targeted to the indicated genes. Mean \pm s.e.m., n=3. p values refer to tests between siLuciferase and indicated siRNA. ** p<0.005, n.s., p>0.05. See Experimental Procedures for analysis of clustering.

(B) Top panels, FISH image of a VA13 cell expressing GFP-Rad51, hybridized with telomeric PNA probe. Last panel shows an expanded area demarcated by the white box. Bottom panels, fluorescence image of a VA13 cell co-expressing mCherry-TRF1-FokI and GFP-Rad51.

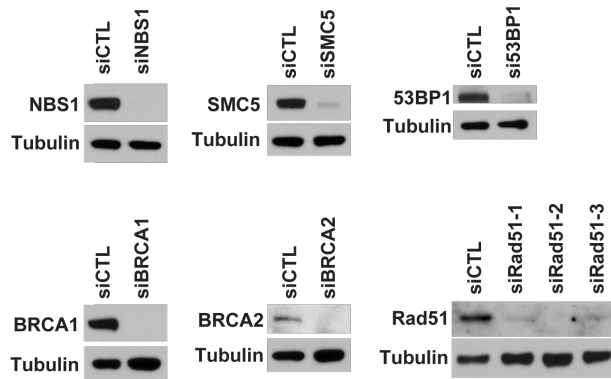
(C) Representative montage of a live-cell telomere clustering event in a VA13 cell expressing mCherry-TRF1-FokI and GFP-Rad51.

(D) MSD analysis of telomere movement after Rad51 knockdown in U2OS cells. Nuclease inactive D450A is shown for reference. Fit determined by a diffusion model, $MSD = \Gamma t^\alpha$. Error bars, weighted s.e.m. and n > 450 tracks from two independent experiments.

(E) Number of telomere clustering events that occur per nucleus following directed movement is quantified after Rad51 knockdown in U2OS cells. Mean \pm s.e.m. from two independent experiments. *** p<0.0005.

Figure 10

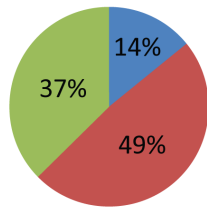
A



B

% of clustering telomeres during live cell imaging

■ No GFP-Rad51 ■ GFP-Rad51 foci ■ GFP-Rad51 filament



C

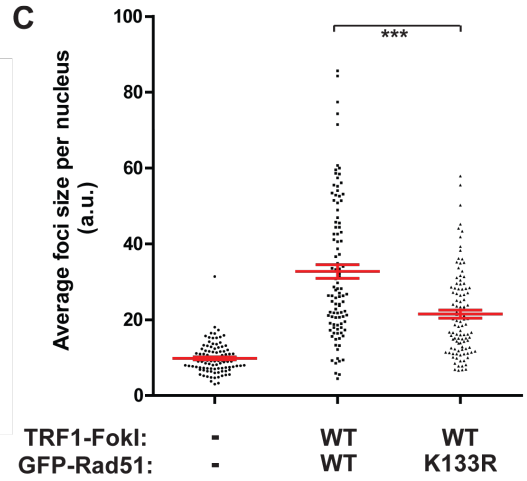


Figure 10. Rad51 Guides ALT Telomere Movement and Clustering

(A) Western blotting was performed in U2OS cells at 72h after knockdown of the indicated genes by siRNA.

(B) Live cell imaging was performed in VA13 cells co-expressing mCherry-TRF1FokI and GFP-Rad51. Cells that contained at least one GFP-Rad51 filament in between telomeres were analyzed for percentages of clustering telomeres that displayed the following characteristics: (1) colocalization with GFP-Rad51 foci, or (2) connected by a GFP-Rad51 filament. n = 35 total clustering events analyzed from 4 independent experiments.

(C) U2OS cells expressing TRF1-FokI WT were transfected with GFP-Rad51 WT or K133R mutant. Average PNA telomeric foci size per nucleus was calculated from >100 cells from three experiments. Mean \pm s.e.m., *** p<0.0005.

Figure 11

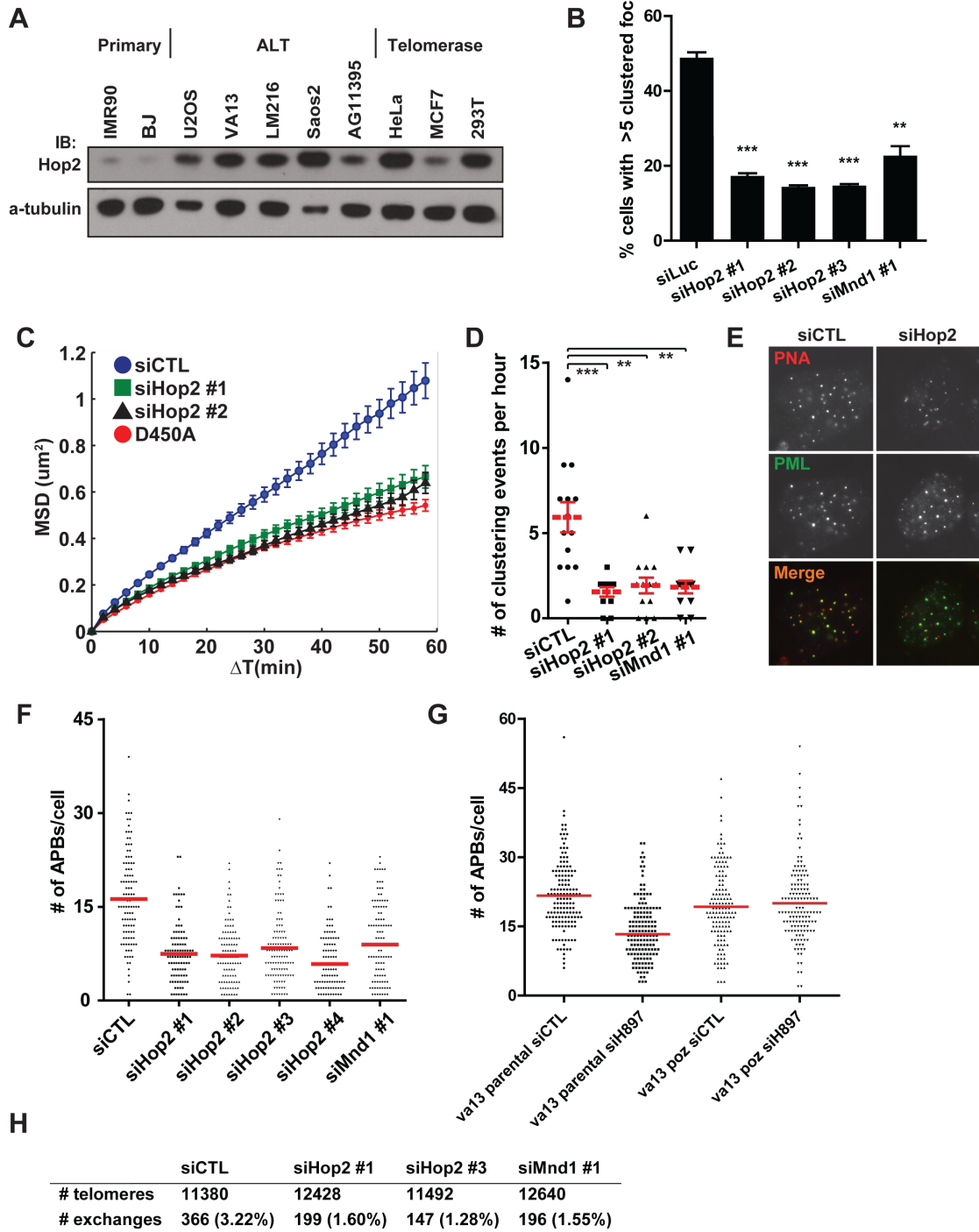


Figure 11. Hop2-Mnd1 Regulate Telomere Clustering and Recombination in ALT

(A) Western blotting was performed in the indicated cell lines using an antibody that recognizes the endogenous Hop2 protein.

(B) Telomere clustering in U2OS cells expressing TRF1-FokI was quantified as in (5A) after Hop2-Mnd1 knockdown. Mean \pm s.e.m., n = 3. ** p<0.005, *** p<0.0005.

(C-D) Live-cell analysis of telomere movement in U2OS cells expressing mCherryTRF1-FokI WT was used to quantify telomere clustering after knockdown with the indicated siRNAs. D450A is shown for reference. Fit determined by $MSD = \Gamma t^\alpha$. Error bars, weighted s.e.m. and n > 550 tracks from two independent experiments. ** p<0.005, *** p<0.0005.

(E) Representative images of telomere colocalization with PML foci in VA13 cells after control or Hop2 knockdown.

(F) Spontaneous APB formation was assessed in VA13 cells after serial knockdown of Hop2 or Mnd1 (Extended Experimental Procedures). Mean from >100 cells from 3 experiments.

(G) Spontaneous APB formation was assessed following Hop2 siRNA targeting the 3' UTR region in parental VA13 cells and in VA13 cells stably expressing Hop2 cDNA. Mean from >100 cells from 3 experiments.

(H) Representative examples of telomere exchanges from CO-FISH are shown for cells with control or Hop2 knockdown (siRNA #1). The arrowhead reveals a T-SCE. Full images shown in Figure S7C.

(I) Quantification of total number of exchanges from CO-FISH assay after Control, Hop2 or Mnd1 knockdown. >50 metaphases in two independent experiments.

Figure 12

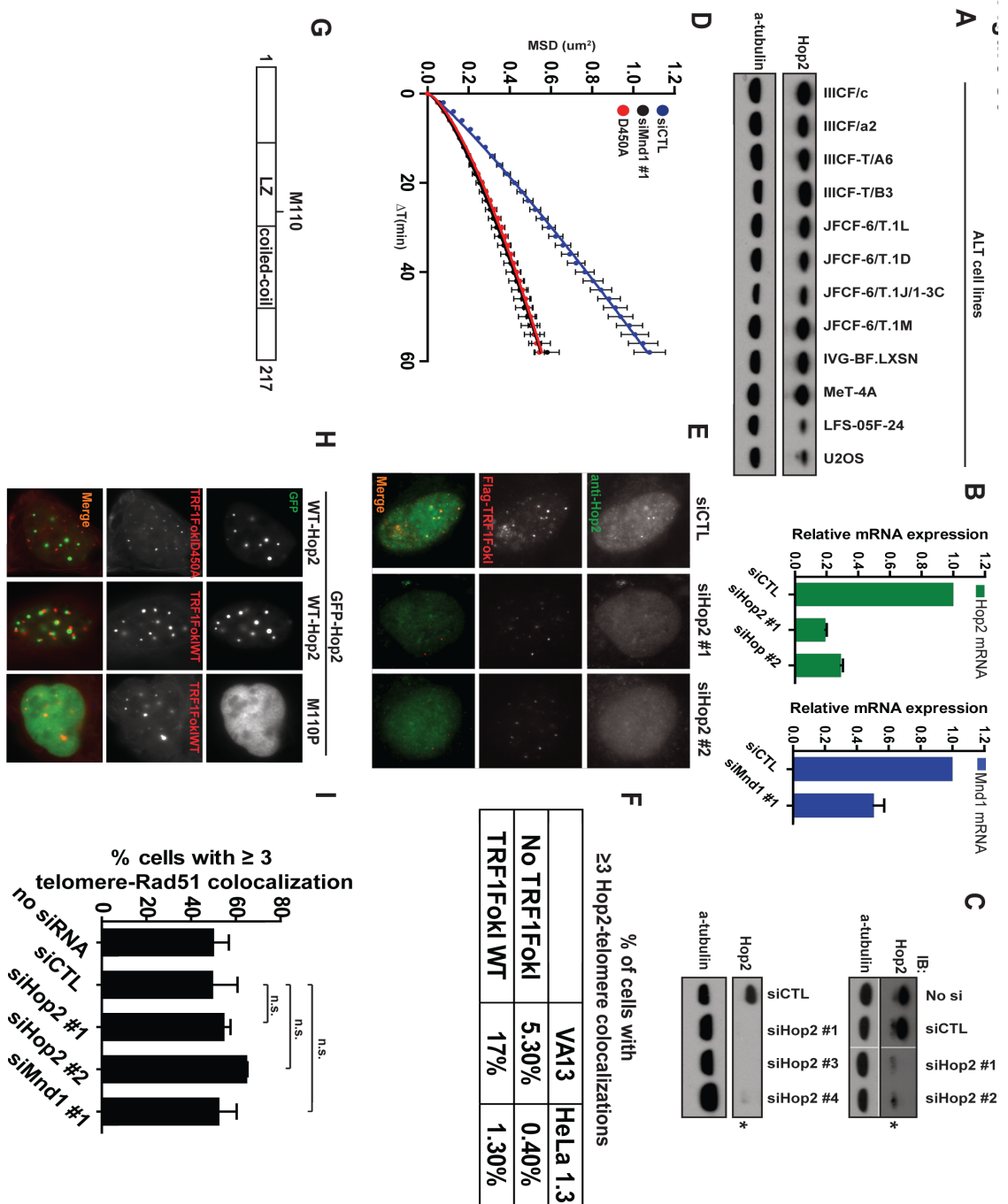


Figure 12. Hop2-Mnd1 Regulates Telomere Clustering and Recombination in ALT.

(A) Western blotting was performed in the indicated ALT cell lines using an antibody that recognizes endogenous Hop2 protein.

(B) Quantitative RT-PCR was performed after transfection of the indicated siRNA in U2OS cells. Mean \pm s.e.m., n=2.

(C) Western blotting was performed using the anti-Hop2 antibody after transfection of the indicated siRNA in U2OS cells. *, nonspecific band seen in longer exposures. White line is shown to indicate irrelevant lanes between siCTL and siHop2 were removed.

(D) Live-cell analysis of telomere movement in U2OS cells expressing mCherryTRF1-FokI WT was used to quantify telomere clustering after knockdown with the indicated siRNAs. D450A is shown for reference. Nonlinear fit determined by a single exponential diffusion model, $MSD = \Gamma t^\alpha$. Error bars, weighted s.e.m. and n > 550 tracks from two independent experiments.

(E) IF was performed in VA13 cells with antibodies to the Flag epitope and to endogenous Hop2 protein as indicated at 72 hours after indicated siRNAs and 24 hours after expression of Flag-TRF1FokI.

(F) Endogenous Hop2 localization to telomeres was quantified in VA13 and HeLa 1.3 cells with or without TRF1-FokI expression.

(G) Schematic of Hop2 protein, highlighting its domain structure and the M110 residue within the Leucine Zipper (LZ) domain.

(H) GFP-Hop2 localization proximal to TRF1-FokI was assessed in U2OS cells. The Leucine Zipper domain mutant, M110P abolished GFP-Hop2 colocalization with TRF1-FokI.

(I) Flag-TRF1FokI WT was expressed in VA13 cells at 48 hours after transfection with the indicated siRNA. Immunofluorescence was performed with anti-Flag and anti-Rad51.

Mean \pm s.e.m, n = 2; n.s., $p > 0.05$.

Figure 13

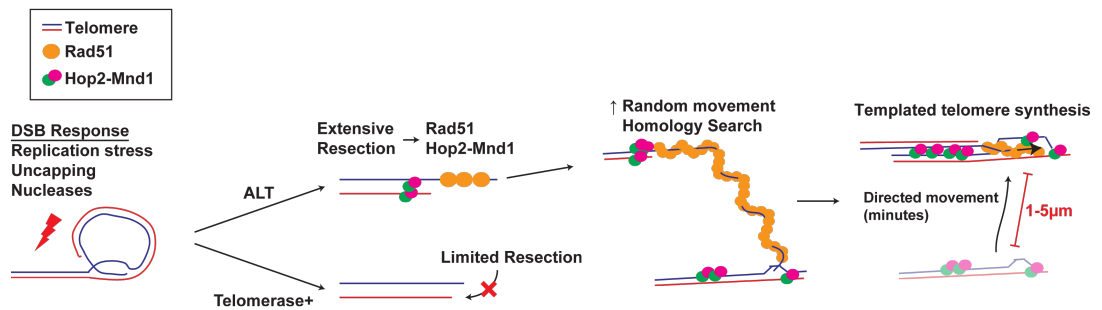


Figure 13. Model for a Specialized Homology Search Mechanism that drives ALT Telomere Recombination

A specialized homology searching mechanism is required for synapsis between distant telomeres. Extensive end resection at ALT telomeres facilitates a Rad51 dependent homology search. Homology capture followed by synapsis and congression of homologously paired non-sister telomeres would be responsible for directional telomere movement. This ALT telomere recombination mechanism relies in part on Rad51 and Hop2-Mnd1 to promote synapsis between non-sister telomeres.

Figure 14

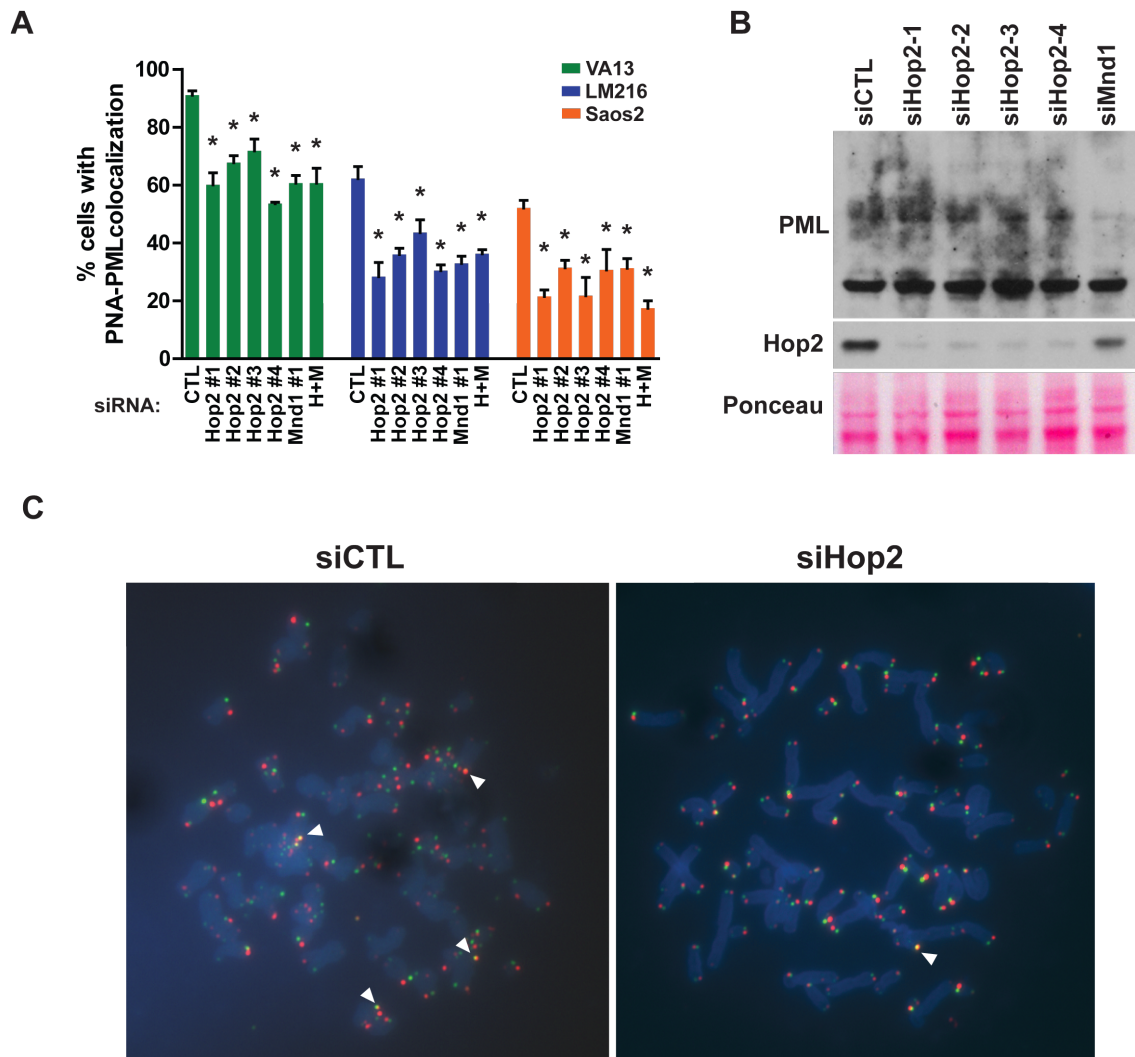


Figure 14. Hop2-Mnd1 Regulates Telomere Clustering and Recombination in ALT.

(A) Spontaneous APB formation was assessed in ALT cell lines with Hop2-Mnd1 depletion. Positive cells exhibited ≥ 3 colocalized foci. siH+M indicates cotransfection of siHop2#1 and Mnd1#1. Mean \pm s.e.m., n = 3. * p<0.05

(B) Western blotting was performed with antibodies to PML or Hop2 in VA13 cells 72 hours after transfection of indicated siRNAs.

(C) Representative images of CO-FISH experiments after knockdown of Hop2. Examples of telomere exchanges are highlighted with white arrowheads.

Figure 15

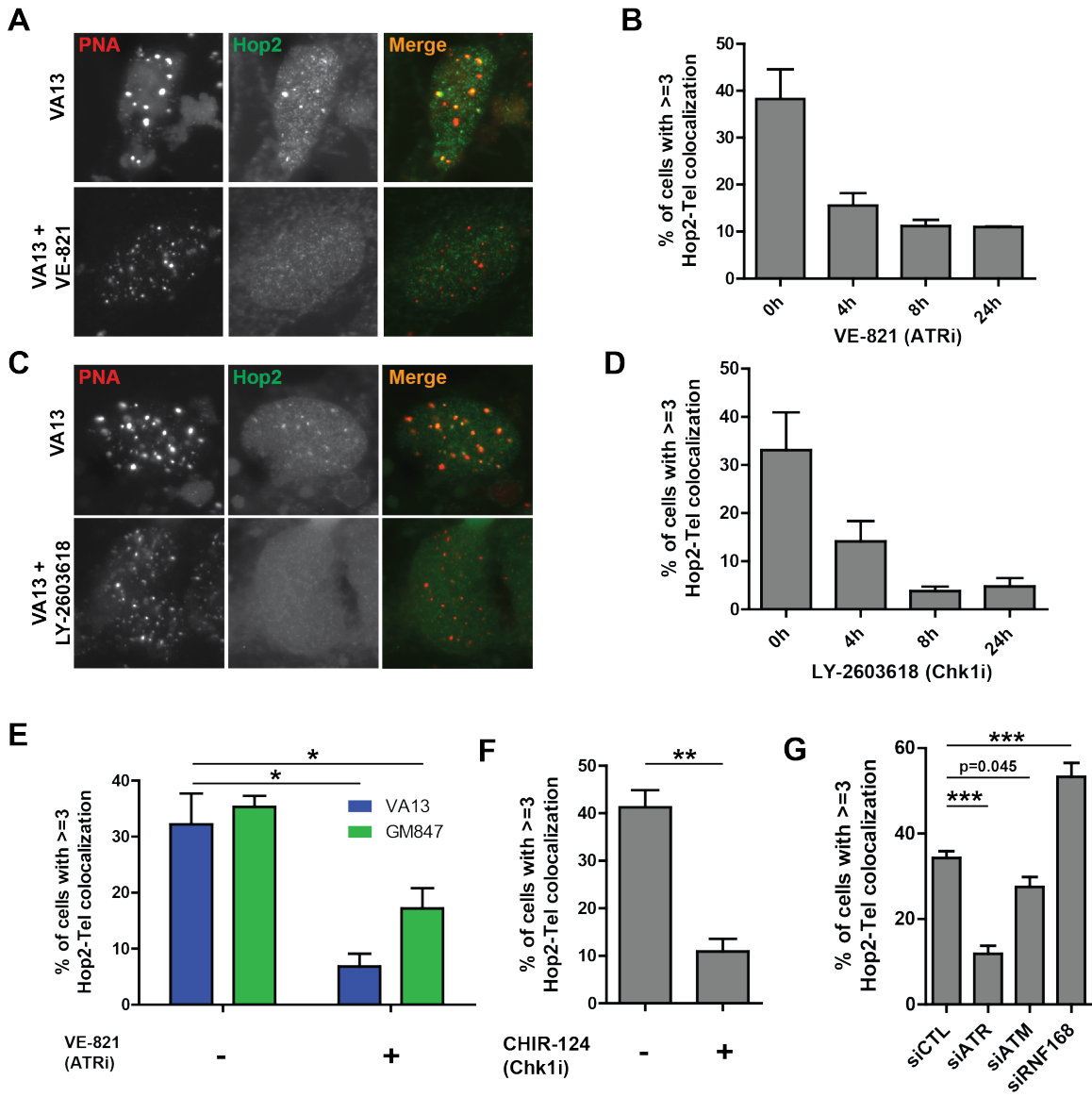


Figure 15. Hop2 localization to telomeres is disrupted upon ATR or Chk1 inhibition.

(A) Representative PNA/Hop2 immuno-FISH images of VA13 cells treated with or without ATR inhibitor (VE-821) for 24h prior to fixation. TRF1-FokI virus was added 24h prior to fixation.

(B) Quantification of Hop2-PNA colocalization events in VA13 cells treated with VE-821 for the indicated durations prior to fixation. TRF1-FokI virus was added 24h prior to fixation. Mean \pm standard error of the mean (s.e.m.) for >50 cells in n = 2.

(C) Representative PNA/Hop2 immuno-FISH images of VA13 cells treated with or without Chk1 inhibitor (LY-2603618) for 24h prior to fixation. TRF1-FokI virus was added 24h prior to fixation.

(D) Quantification of Hop2-PNA colocalization events in VA13 cells treated with LY-2603618 for the indicated durations prior to fixation. TRF1-FokI virus was added 24h prior to fixation. Mean \pm standard error of the mean (s.e.m.) for >50 cells in n = 2.

(E) Quantification of Hop2-PNA colocalization in VA13 and GM847 ALT cells treated with or without VE-821 for 24h prior to fixation. TRF1-FokI virus was added 24h prior to fixation. Mean \pm standard error of the mean (s.e.m.) for >50 cells in n = 2. * p<0.05

(F) Quantification of Hop2-PNA colocalization in VA13 cells treated with or without Chk1 inhibitor (CHIR-124) for 24h prior to fixation. TRF1-FokI virus was added 24h

prior to fixation. Mean \pm standard error of the mean (s.e.m.) for >50 cells in n = 2. **
p<0.005

(G) Quantification of Hop2-PNA colocalization in VA13 cells transfected with the indicated siRNAs. TRF1-FokI virus was added 24h prior to fixation. Mean \pm standard error of the mean (s.e.m.) for >50 cells in n = 3. *** p<0.0005

Figure 16

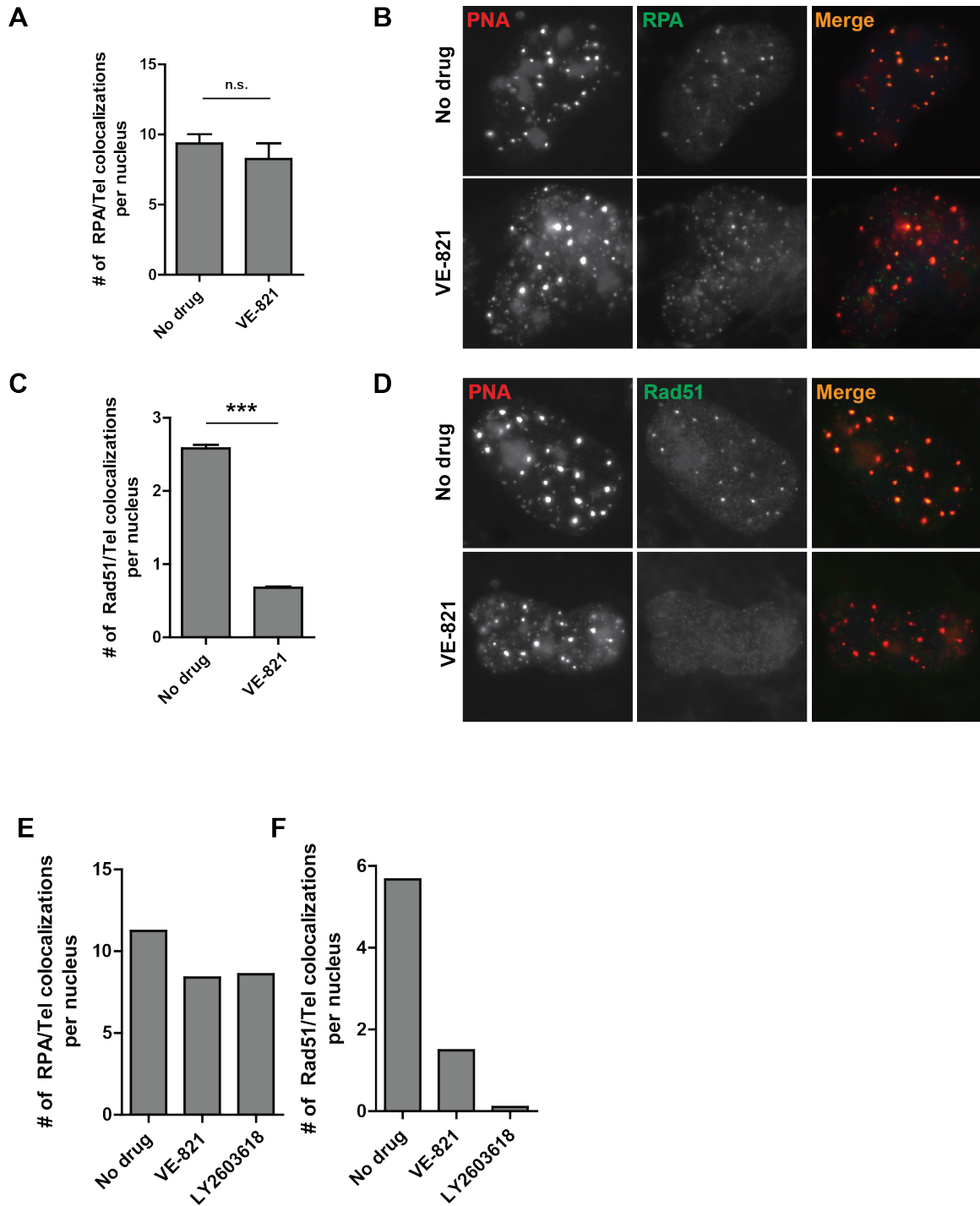


Figure 16. ATR and Chk1 inhibition reduces Rad51, but not RPA, localization to ALT telomeres.

(A) Quantification of RPA/PNA colocalization events in VA13 cells treated with or without VE-821 for 24h. Mean \pm standard error of the mean (s.e.m.) for >50 cells in n = 3. n.s. $p > 0.05$.

(B) Representative RPA/PNA immuno-FISH images of VA13 cells treated with or without VE-821 for 24h.

(C) Quantification of Rad51/PNA colocalization events in VA13 cells treated with or without VE-821 for 24h. Mean \pm standard error of the mean (s.e.m.) for >50 cells in n = 3. n.s. $p > 0.05$.

(D) Representative Rad51/PNA immuno-FISH images of VA13 cells treated with or without VE-821 for 24h.

(E) Quantification of RPA/PNA colocalization events in U2OS cells treated with or without VE-821 for 24h. TRF1-FokI virus was added 24h prior to fixation.

(F) Quantification of Rad51/PNA colocalization events in U2OS cells treated with or without VE-821 for 24h. TRF1-FokI virus was added 24h prior to fixation.

Figure 17

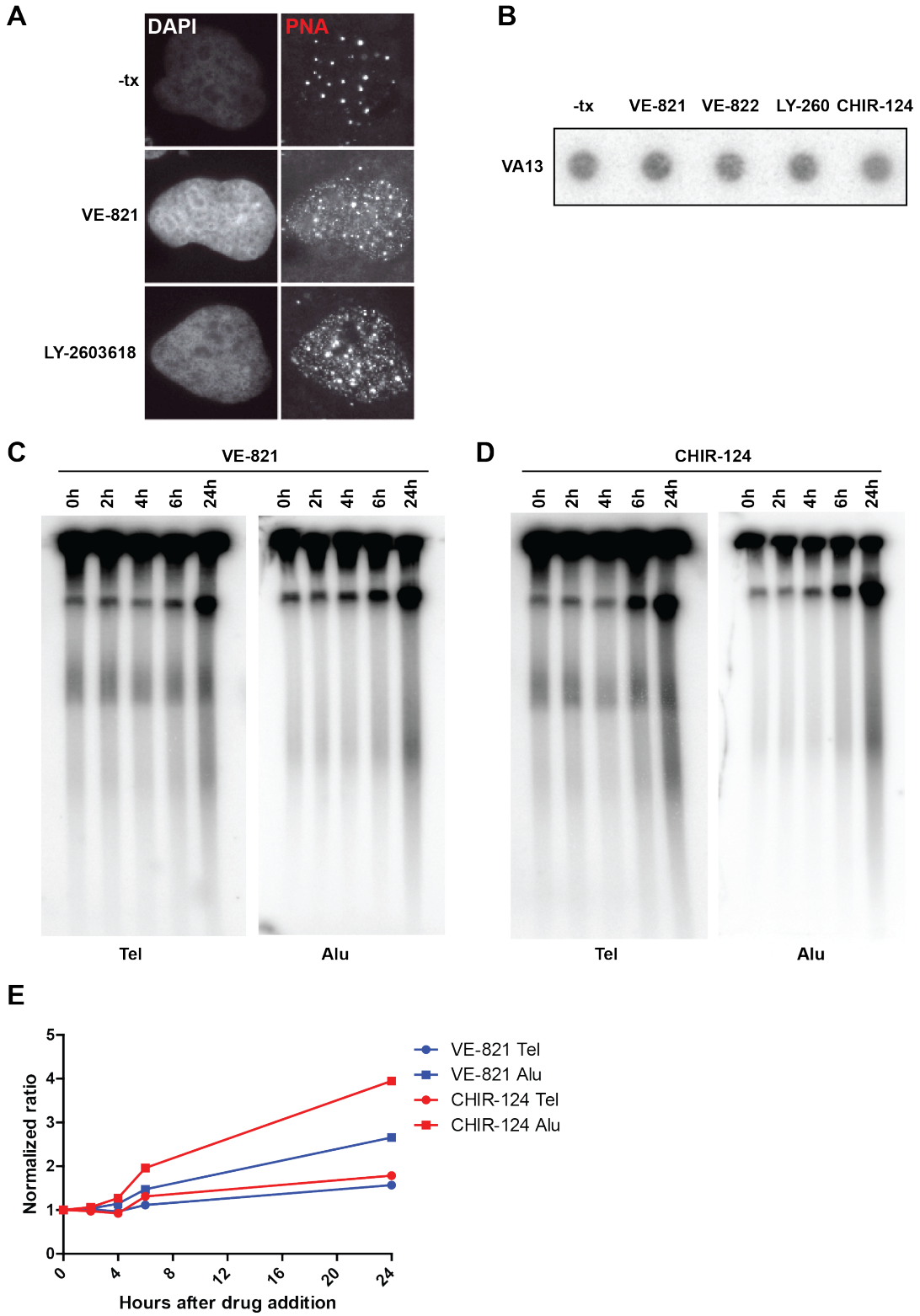


Figure 17. Genome fragmentation occurs following ATR or Chk1 inhibition.

(A) Representative PNA FISH images of VA13 cells treated with ATRi (VE-821) or Chk1i (LY-2603618).

(B) C-circle assay was performed on genomic DNA isolated from VA13 cells treated with the indicated drugs.

(C) VA13 cells treated with the indicated durations of VE-821 were embedded in agarose plugs and electrophoresed to visualize fragmented DNA with the indicated probes (Tel, 6xCCCTAA; Alu, alu-repeat specific).

(D) VA13 cells treated with the indicated durations of CHIR-124 were embedded in agarose plugs and electrophoresed to visualize fragmented DNA with the indicated probes (Tel, 6xCCCTAA; Alu, alu-repeat specific).

(E) Quantification of lane intensity was performed using ImageJ. Values were normalized to the intensity of 0h time point.

Figure 18

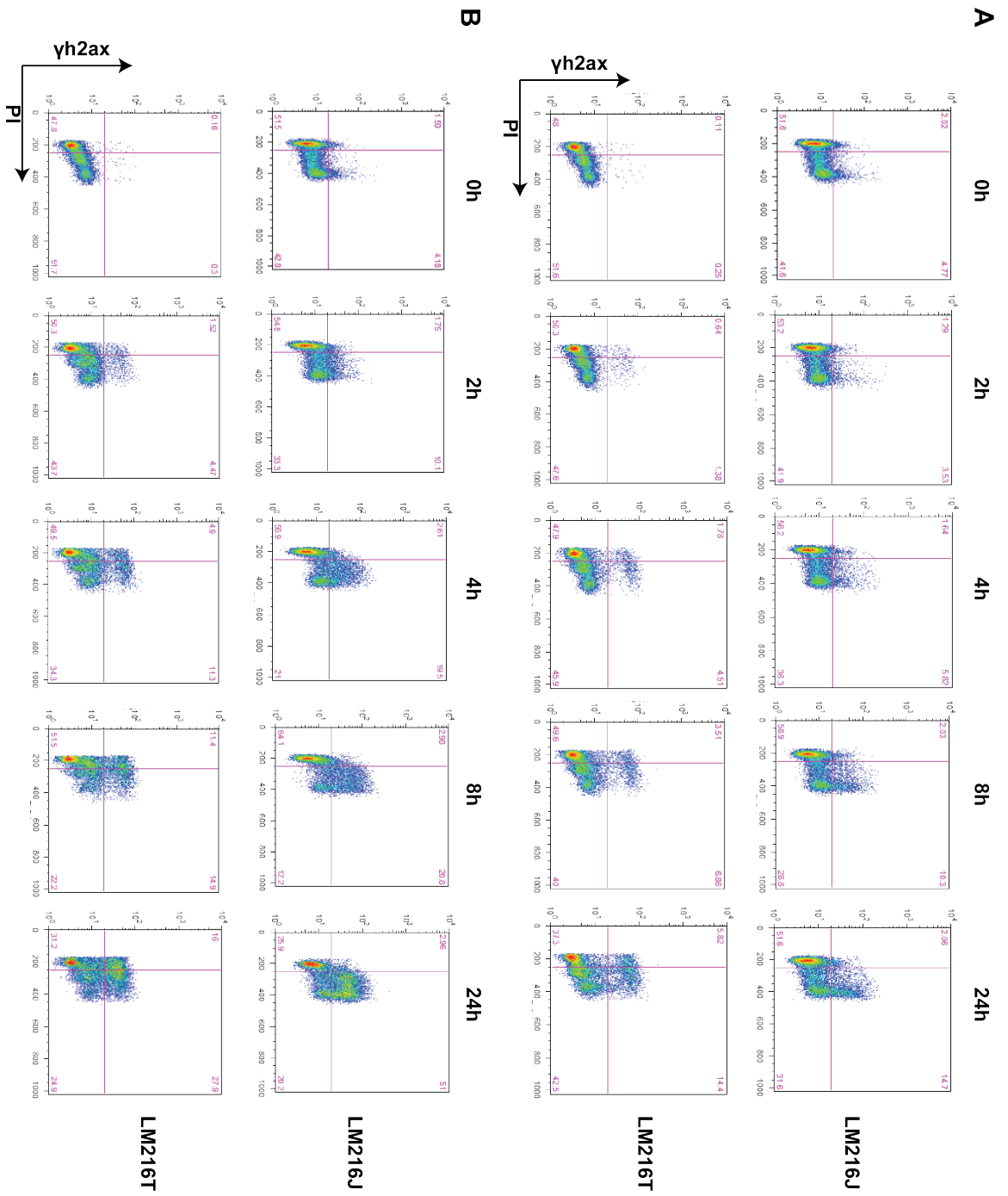


Figure 18. γ H2Ax is increased following ATR or Chk1 inhibition in LM216^{ALT} and LM216^{TEL} cells.

(A) LM216^{ALT} and LM216^{TEL} cells were incubated with VE-821 for the indicated durations, stained for γ H2Ax and PI, and analyzed by flow cytometry.

(B) LM216^{ALT} and LM216^{TEL} cells were incubated with CHIR-124 for the indicated durations, stained for γ H2Ax and PI, and analyzed by flow cytometry.

Figure 19

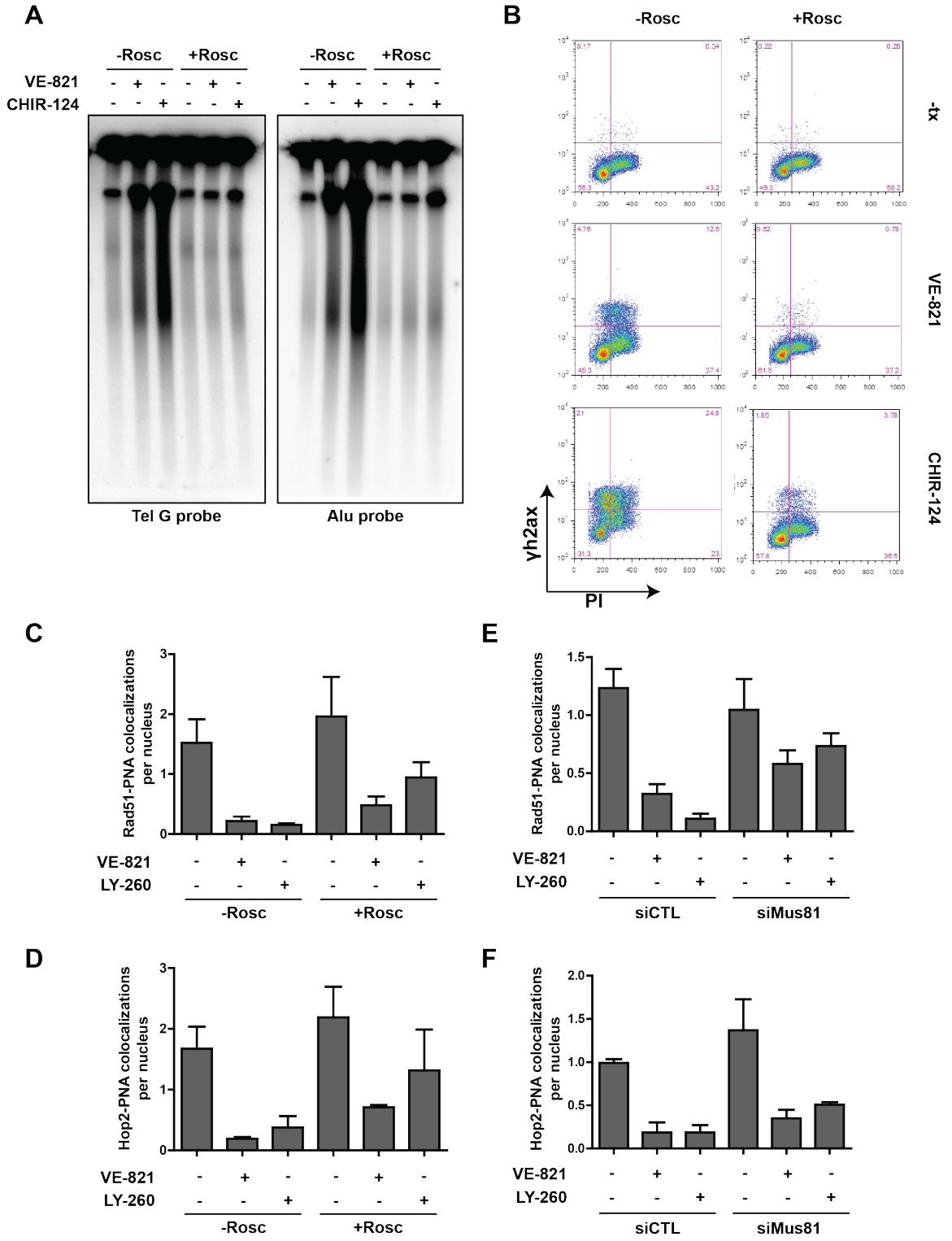


Figure 19. Roscovitine and Mus81 knockdown rescues the effects of ATRi and Chk1i.

(A) VA13 cells treated with the indicated drugs for 24h were embedded in agarose plugs and electrophoresed to visualize fragmented DNA with the indicated probes (Tel, 6xCCCTAA; Alu, alu-repeat specific).

(B) VA13 cells treated with the indicated drugs for 24h were stained for γ H2Ax and PI, and analyzed by flow cytometry.

(C-D) Rad51/PNA and Hop2/PNA colocalization events were quantified in VA13 cells treated with the indicated drugs for 24h. For Hop2 analysis, TRF1-FokI virus was added 24h prior to fixation. LY260 represents LY-2603618.

(E-F) Rad51/PNA and Hop2/PNA colocalization events were quantified in VA13 cells transfected with control or Mus81 siRNA and treated with the indicated drugs for 24h. For Hop2 analysis, TRF1-FokI virus was added 24h prior to fixation. LY260 represents LY-2603618.

Figure 20

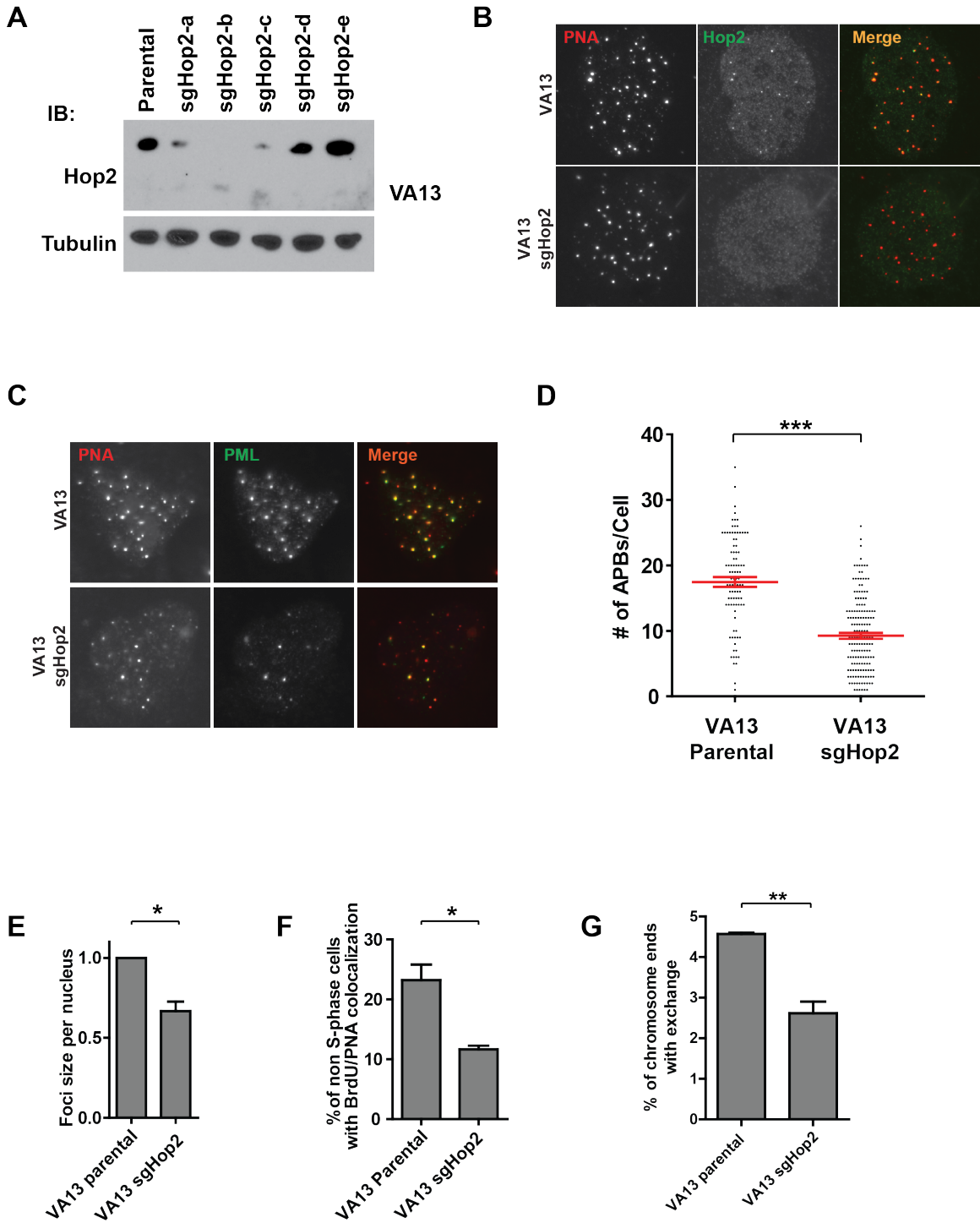


Figure 20. CRISPR-Cas9 mediated deletion of Hop2 suppress ALT phenotypes

(A) Western blotting was performed in VA13 cells selected for expression of the indicated guide RNAs (sgHop2 a-e).

(B) Representative PNA/Hop2 immuno-FISH images of VA13 parental cells and VA13 cells expressing sgHop2-b.

(C) Representative PNA/PML immuno-FISH images of VA13 parental cells and VA13 cells expressing sgHop2-b.

(D) Number of PML-PNA colocalizations (APBs) per nucleus was quantified in VA13 parental cells and VA13 sgHop2-b cells. *** $p < 0.005$

(E) Average PNA foci size per nucleus was quantified in VA13 parental cells and VA13 sgHop2-b cells. * $p < 0.05$

(F) After a BrdU pulse of 2h, % of cells outside of S phase that contained >2 BrdU-PNA colocalizations was quantified in VA13 parental cells and VA13 sgHop2-b cells. * $p < 0.05$

(G) Total number of signal exchanges from CO-FISH assay was quantified in VA13 parental cells and VA13 sgHop2-b cells. ** $p < 0.005$

Movies

Movie 1. Live cell imaging of telomeres after DSB induction demonstrates movement and clustering. Representative U2OS nucleus expressing mCherry-ER-DD-TRF1-FokIWT, Cells were induced for 60 minutes with 4-OHT and Shield1 ligand, then imaged for the following 60 minutes. Z stacks of mCherry signals were acquired every 2 minutes, and each frame represents the stack as a projection onto a single plane. mCherry signals appear in white, while the colored lines track the path traveled by the mCherry focus.

Movie 2. Live cell imaging of telomeres in the absence of DSBs. Representative U2OS nucleus expressing the nuclease-inactive mCherry-ER-DD-TRF1-FokID450A. Cells were induced for 60 minutes with 4-OHT and Shield1 ligand, then imaged for the following 60 minutes. Z stacks of mCherry signals were acquired every 2 minutes, and each frame represents the stack as a projection onto a single plane. mCherry signals appear in white, while the colored lines track the path traveled by the mCherry focus.

Movie 3. Example of spontaneous telomere clustering. Representative U2OS cell nucleus with induction of the mCherry-ER-DD-TRF1 only protein by 4-OHT and Shield1 ligand. Images were acquired as Z stacks every 2 minutes, and each frame represents the stack as a projection onto a single plane. White box highlights a spontaneous telomere association event.

Movie 4. Live cell imaging of mCherry-TRF1FokI foci and interconnecting GFP-Rad51 filaments in a VA13 cell. An example of a telomere clustering event with an

interconnecting GFP-Rad51 filament. Images were acquired as Z stacks every 4 minutes, and each frame represents the stack as a projection onto a single plane.

Movie 5. Live cell imaging of telomeres in U2OS transfected with control siRNA.

mCherry-ER-DD-TRF1-FokI WT was transfected at 48h following transfection with control siRNA and imaging performed 16 hours later. Cells were induced for 60 minutes with 4-OHT and Shield1 ligand, then imaged for the following 60 minutes. Z stacks of mCherry signals were acquired every 2 minutes, and each frame represents the stack as a projection onto a single plane.

Movie 6. Live cell imaging of telomeres in U2OS transfected with siRNA targeted to

Rad51 demonstrates reduced movement. mCherry-ER-DD-TRF1-FokI WT was transfected at 48h following transfection with siRad51 #2, and imaging performed 16 hours later. Cells were induced for 60 minutes with 4-OHT and Shield1 ligand, then imaged for the following 60 minutes. Z stacks of mCherry signals were acquired every 2 minutes, and each frame represents the stack as a projection onto a single plane.

Movie 7. Live cell imaging of telomeres in U2OS transfected with siRNA targeted to

Hop2 demonstrates reduced movement. mCherry-ER-DD-TRF1-FokI WT was transfected at 48h following transfection with siHop2 #2, and imaging performed 16 hours later. Cells were induced for 60 minutes with 4-OHT and Shield1 ligand, then imaged for the following 60 minutes. Z stacks of mCherry signals were acquired every 2 minutes, and each frame represents the stack as a projection onto a single plane.

BIBLIOGRAPHY

1. Aten, J.A., Stap, J., Krawczyk, P.M., van Oven, C.H., Hoebe, R.A., Essers, J., and Kanaar, R. (2004). Dynamics of DNA double-strand breaks revealed by clustering of damaged chromosome domains. *Science* 303, 92-95.
2. Aylon, Y., Liefshitz, B., and Kupiec, M. (2004). The CDK regulates repair of double-strand breaks by homologous recombination during the cell cycle. *The EMBO journal* 23, 4868-4875.
3. Bailey, S.M., Brenneman, M.A., and Goodwin, E.H. (2004). Frequent recombination in telomeric DNA may extend the proliferative life of telomerase-negative cells. *Nucleic acids research* 32, 3743-3751.
4. Ball, H.L., Myers, J.S., and Cortez, D. (2005). ATRIP binding to replication protein A-single-stranded DNA promotes ATR-ATRIP localization but is dispensable for Chk1 phosphorylation. *Mol Biol Cell* 16, 2372-2381.
5. Bechter, O.E., Zou, Y., Shay, J.W., and Wright, W.E. (2003). Homologous recombination in human telomerase-positive and ALT cells occurs with the same frequency. *EMBO reports* 4, 1138-1143.
6. Bishop, D.K. (1994). RecA homologues Dmc1 and Rad51 interact to form multiple nuclear complexes prior to meiotic chromosome synapsis. *Cell* 79, 1081-1092.
7. Bouwman, P., Aly, A., Escandell, J.M., Pieterse, M., Bartkova, J., van der Gulden, H., Hiddingh, S., Thanasoula, M., Kulkarni, A., Yang, Q., *et al.* (2010). 53BP1 loss rescues BRCA1 deficiency and is associated with triple-negative and BRCA-mutated breast cancers. *Nature structural & molecular biology* 17, 688-695.

8. Bugreev, D.V., Huang, F., Mazina, O.M., Pezza, R.J., Voloshin, O.N., Daniel Camerini-Otero, R., and Mazin, A.V. (2014). HOP2-MND1 modulates RAD51 binding to nucleotides and DNA. *Nature communications* 5, 4198.
9. Buisson, R., Boisvert, J.L., Benes, C.H., and Zou, L. (2015). Distinct but Concerted Roles of ATR, DNA-PK, and Chk1 in Countering Replication Stress during S Phase. *Molecular cell* 59, 1011-1024.
10. Bunting, S.F., Callen, E., Wong, N., Chen, H.T., Polato, F., Gunn, A., Bothmer, A., Feldhahn, N., Fernandez-Capetillo, O., Cao, L., *et al.* (2010). 53BP1 inhibits homologous recombination in Brca1-deficient cells by blocking resection of DNA breaks. *Cell* 141, 243-254.
11. Cerone, M.A., Autexier, C., Londono-Vallejo, J.A., and Bacchetti, S. (2005). A human cell line that maintains telomeres in the absence of telomerase and of key markers of ALT. *Oncogene* 24, 7893-7901.
12. Cerone, M.A., Londono-Vallejo, J.A., and Bacchetti, S. (2001). Telomere maintenance by telomerase and by recombination can coexist in human cells. *Hum Mol Genet* 10, 1945-1952.
13. Cesare, A.J., and Griffith, J.D. (2004). Telomeric DNA in ALT cells is characterized by free telomeric circles and heterogeneous t-loops. *Molecular and cellular biology* 24, 9948-9957.
14. Cesare, A.J., Hayashi, M.T., Crabbe, L., and Karlseder, J. (2013). The telomere deprotection response is functionally distinct from the genomic DNA damage response. *Molecular cell* 51, 141-155.

15. Cesare, A.J., and Karlseder, J. (2012). A three-state model of telomere control over human proliferative boundaries. *Current opinion in cell biology* *24*, 731-738.
16. Cesare, A.J., Kaul, Z., Cohen, S.B., Napier, C.E., Pickett, H.A., Neumann, A.A., and Reddel, R.R. (2009). Spontaneous occurrence of telomeric DNA damage response in the absence of chromosome fusions. *Nature structural & molecular biology* *16*, 1244-1251.
17. Chapman, J.R., Sossick, A.J., Boulton, S.J., and Jackson, S.P. (2012). BRCA1-associated exclusion of 53BP1 from DNA damage sites underlies temporal control of DNA repair. *Journal of cell science* *125*, 3529-3534.
18. Chen, B., Gilbert, L.A., Cimini, B.A., Schnitzbauer, J., Zhang, W., Li, G.W., Park, J., Blackburn, E.H., Weissman, J.S., Qi, L.S., *et al.* (2013). Dynamic imaging of genomic loci in living human cells by an optimized CRISPR/Cas system. *Cell* *155*, 1479-1491.
19. Chen, Q., Ijima, A., and Greider, C.W. (2001). Two survivor pathways that allow growth in the absence of telomerase are generated by distinct telomere recombination events. *Molecular and cellular biology* *21*, 1819-1827.
20. Chen, Z., Yang, H., and Pavletich, N.P. (2008). Mechanism of homologous recombination from the RecA-ssDNA/dsDNA structures. *Nature* *453*, 489-484.
21. Chi, P., San Filippo, J., Sehorn, M.G., Petukhova, G.V., and Sung, P. (2007). Bipartite stimulatory action of the Hop2-Mnd1 complex on the Rad51 recombinase. *Genes & development* *21*, 1747-1757.

22. Chung, I., Leonhardt, H., and Rippe, K. (2011). De novo assembly of a PML nuclear subcompartment occurs through multiple pathways and induces telomere elongation. *Journal of cell science* *124*, 3603-3618.
23. Clynes, D., Jelinska, C., Xella, B., Ayyub, H., Scott, C., Mitson, M., Taylor, S., Higgs, D.R., and Gibbons, R.J. (2015). Suppression of the alternative lengthening of telomere pathway by the chromatin remodelling factor ATRX. *Nat Commun* *6*, 7538.
24. Cobb, J.A., Bjergbaek, L., Shimada, K., Frei, C., and Gasser, S.M. (2003). DNA polymerase stabilization at stalled replication forks requires Mec1 and the RecQ helicase Sgs1. *Embo J* *22*, 4325-4336.
25. Cohen, H., and Sinclair, D.A. (2001). Recombination-mediated lengthening of terminal telomeric repeats requires the Sgs1 DNA helicase. *Proceedings of the National Academy of Sciences of the United States of America* *98*, 3174-3179.
26. Conomos, D., Reddel, R.R., and Pickett, H.A. (2014). NuRD-ZNF827 recruitment to telomeres creates a molecular scaffold for homologous recombination. *Nat Struct Mol Biol* *21*, 760-770.
27. Costantino, L., Sotiriou, S.K., Rantala, J.K., Magin, S., Mladenov, E., Helleday, T., Haber, J.E., Iliakis, G., Kallioniemi, O.P., and Halazonetis, T.D. (2014). Break-induced replication repair of damaged forks induces genomic duplications in human cells. *Science* *343*, 88-91.
28. de Lange, T. (2005). Shelterin: the protein complex that shapes and safeguards human telomeres. *Genes Dev* *19*, 2100-2110.

29. Dellaire, G., and Bazett-Jones, D.P. (2004). PML nuclear bodies: dynamic sensors of DNA damage and cellular stress. *Bioessays* *26*, 963-977.
30. Dimitrova, N., Chen, Y.C., Spector, D.L., and de Lange, T. (2008). 53BP1 promotes non-homologous end joining of telomeres by increasing chromatin mobility. *Nature* *456*, 524-528.
31. Dion, V., Kalck, V., Horigome, C., Towbin, B.D., and Gasser, S.M. (2012). Increased mobility of double-strand breaks requires Mec1, Rad9 and the homologous recombination machinery. *Nature cell biology* *14*, 502-509.
32. Doe, C.L., Ahn, J.S., Dixon, J., and Whitby, M.C. (2002). Mus81-Eme1 and Rqh1 involvement in processing stalled and collapsed replication forks. *J Biol Chem* *277*, 32753-32759.
33. Donnianni, R.A., and Symington, L.S. (2013). Break-induced replication occurs by conservative DNA synthesis. *Proc Natl Acad Sci U S A* *110*, 13475-13480.
34. Draskovic, I., Arnoult, N., Steiner, V., Bacchetti, S., Lomonte, P., and Londono-Vallejo, A. (2009). Probing PML body function in ALT cells reveals spatiotemporal requirements for telomere recombination. *Proceedings of the National Academy of Sciences of the United States of America* *106*, 15726-15731.
35. Dunham, M.A., Neumann, A.A., Fasching, C.L., and Reddel, R.R. (2000). Telomere maintenance by recombination in human cells. *Nat Genet* *26*, 447-450.
36. Falck, J., Mailand, N., Syljuasen, R.G., Bartek, J., and Lukas, J. (2001). The ATM-Chk2-Cdc25A checkpoint pathway guards against radioresistant DNA synthesis. *Nature* *410*, 842-847.

37. Fasching, C.L., Bower, K., and Reddel, R.R. (2005). Telomerase-independent telomere length maintenance in the absence of alternative lengthening of telomeres-associated promyelocytic leukemia bodies. *Cancer Res* 65, 2722-2729.
38. Fasching, C.L., Neumann, A.A., Muntoni, A., Yeager, T.R., and Reddel, R.R. (2007). DNA damage induces alternative lengthening of telomeres (ALT) associated promyelocytic leukemia bodies that preferentially associate with linear telomeric DNA. *Cancer research* 67, 7072-7077.
39. Flynn, R.L., Cox, K.E., Jeitany, M., Wakimoto, H., Bryll, A.R., Ganem, N.J., Bersani, F., Pineda, J.R., Suva, M.L., Benes, C.H., *et al.* (2015). Alternative lengthening of telomeres renders cancer cells hypersensitive to ATR inhibitors. *Science* 347, 273-277.
40. Flynn, R.L., and Zou, L. (2011). ATR: a master conductor of cellular responses to DNA replication stress. *Trends Biochem Sci* 36, 133-140.
41. Greider, C.W., and Blackburn, E.H. (1985). Identification of a specific telomere terminal transferase activity in Tetrahymena extracts. *Cell* 43, 405-413.
42. Griffith, J.D., Comeau, L., Rosenfield, S., Stansel, R.M., Bianchi, A., Moss, H., and de Lange, T. (1999). Mammalian telomeres end in a large duplex loop. *Cell* 97, 503-514.
43. Guigas, G., and Weiss, M. (2008). Sampling the cell with anomalous diffusion - the discovery of slowness. *Biophysical journal* 94, 90-94.
44. Hayashi, M.T., Cesare, A.J., Rivera, T., and Karlseder, J. (2015). Cell death during crisis is mediated by mitotic telomere deprotection. *Nature* 522, 492-496.

45. Heaphy, C.M., de Wilde, R.F., Jiao, Y., Klein, A.P., Edil, B.H., Shi, C., Bettgowda, C., Rodriguez, F.J., Eberhart, C.G., Hebbar, S., *et al.* (2011). Altered telomeres in tumors with ATRX and DAXX mutations. *Science* 333, 425.
46. Henson, J.D., Cao, Y., Huschtscha, L.I., Chang, A.C., Au, A.Y., Pickett, H.A., and Reddel, R.R. (2009). DNA C-circles are specific and quantifiable markers of alternative-lengthening-of-telomeres activity. *Nature biotechnology* 27, 1181-1185.
47. Hu, J., Hwang, S.S., Liesa, M., Gan, B., Sahin, E., Jaskelioff, M., Ding, Z., Ying, H., Boutin, A.T., Zhang, H., *et al.* (2012). Antitelomerase therapy provokes ALT and mitochondrial adaptive mechanisms in cancer. *Cell* 148, 651-663.
48. Huang, P., Pryde, F.E., Lester, D., Maddison, R.L., Borts, R.H., Hickson, I.D., and Louis, E.J. (2001). SGS1 is required for telomere elongation in the absence of telomerase. *Current biology : CB* 11, 125-129.
49. Huertas, P., Cortes-Ledesma, F., Sartori, A.A., Aguilera, A., and Jackson, S.P. (2008). CDK targets Sae2 to control DNA-end resection and homologous recombination. *Nature* 455, 689-692.
50. Ira, G., and Haber, J.E. (2002). Characterization of RAD51-independent break-induced replication that acts preferentially with short homologous sequences. *Molecular and cellular biology* 22, 6384-6392.
51. Ira, G., Pellicioli, A., Balijja, A., Wang, X., Fiorani, S., Carotenuto, W., Liberi, G., Bressan, D., Wan, L., Hollingsworth, N.M., *et al.* (2004). DNA end resection, homologous recombination and DNA damage checkpoint activation require CDK1. *Nature* 431, 1011-1017.

52. Jegou, T., Chung, I., Heuvelman, G., Wachsmuth, M., Gorisch, S.M., Greulich-Bode, K.M., Boukamp, P., Lichter, P., and Rippe, K. (2009). Dynamics of telomeres and promyelocytic leukemia nuclear bodies in a telomerase-negative human cell line. *Molecular biology of the cell* 20, 2070-2082.
53. Jiang, W.Q., Zhong, Z.H., Henson, J.D., Neumann, A.A., Chang, A.C., and Reddel, R.R. (2005). Suppression of alternative lengthening of telomeres by Sp100-mediated sequestration of the MRE11/RAD50/NBS1 complex. *Mol Cell Biol* 25, 2708-2721.
54. Jiang, W.Q., Zhong, Z.H., Henson, J.D., and Reddel, R.R. (2007). Identification of candidate alternative lengthening of telomeres genes by methionine restriction and RNA interference. *Oncogene* 26, 4635-4647.
55. Johnson, F.B., Marciniak, R.A., McVey, M., Stewart, S.A., Hahn, W.C., and Guarente, L. (2001). The *Saccharomyces cerevisiae* WRN homolog Sgs1p participates in telomere maintenance in cells lacking telomerase. *Embo J* 20, 905-913.
56. Johnson, R.D., and Jasin, M. (2000). Sister chromatid gene conversion is a prominent double-strand break repair pathway in mammalian cells. *Embo J* 19, 3398-3407.
57. Kalocsay, M., Hiller, N.J., and Jentsch, S. (2009). Chromosome-wide Rad51 spreading and SUMO-H2A.Z-dependent chromosome fixation in response to a persistent DNA double-strand break. *Molecular cell* 33, 335-343.
58. Kidane, D., Jonason, A.S., Gorton, T.S., Mihaylov, I., Pan, J., Keeney, S., de Rooij, D.G., Ashley, T., Keh, A., Liu, Y., *et al.* (2010). DNA polymerase beta is critical for mouse meiotic synapsis. *Embo J* 29, 410-423.

59. Komosa, M., Root, H., and Meyn, M.S. (2015). Visualization and quantitative analysis of extrachromosomal telomere-repeat DNA in individual human cells by Halo-FISH. *Nucleic Acids Res* *43*, 2152-2163.
60. Krawczyk, P.M., Borovski, T., Stap, J., Cijssouw, T., ten Cate, R., Medema, J.P., Kanaar, R., Franken, N.A., and Aten, J.A. (2012). Chromatin mobility is increased at sites of DNA double-strand breaks. *Journal of cell science* *125*, 2127-2133.
61. Le, S., Moore, J.K., Haber, J.E., and Greider, C.W. (1999). RAD50 and RAD51 define two pathways that collaborate to maintain telomeres in the absence of telomerase. *Genetics* *152*, 143-152.
62. Lesterlin, C., Ball, G., Schermelleh, L., and Sherratt, D.J. (2013). RecA bundles mediate homology pairing between distant sisters during DNA break repair. *Nature*.
63. Leu, J.Y., Chua, P.R., and Roeder, G.S. (1998). The meiosis-specific Hop2 protein of *S. cerevisiae* ensures synapsis between homologous chromosomes. *Cell* *94*, 375-386.
64. Liu, Q., Guntuku, S., Cui, X.S., Matsuoka, S., Cortez, D., Tamai, K., Luo, G., Carattini-Rivera, S., DeMayo, F., Bradley, A., *et al.* (2000). Chk1 is an essential kinase that is regulated by Atr and required for the G(2)/M DNA damage checkpoint. *Genes Dev* *14*, 1448-1459.
65. Londono-Vallejo, J.A., Der-Sarkissian, H., Cazes, L., Bacchetti, S., and Reddel, R.R. (2004). Alternative lengthening of telomeres is characterized by high rates of telomeric exchange. *Cancer Res* *64*, 2324-2327.

66. Louis, E.J., Naumova, E.S., Lee, A., Naumov, G., and Haber, J.E. (1994). The chromosome end in yeast: its mosaic nature and influence on recombinational dynamics. *Genetics* *136*, 789-802.
67. Lovejoy, C.A., Li, W., Reisenweber, S., Thongthip, S., Bruno, J., de Lange, T., De, S., Petrini, J.H., Sung, P.A., Jasin, M., *et al.* (2012). Loss of ATRX, genome instability, and an altered DNA damage response are hallmarks of the alternative lengthening of telomeres pathway. *PLoS genetics* *8*, e1002772.
68. Lucca, C., Vanoli, F., Cotta-Ramusino, C., Pelliccioli, A., Liberi, G., Haber, J., and Foiani, M. (2004). Checkpoint-mediated control of replisome-fork association and signalling in response to replication pausing. *Oncogene* *23*, 1206-1213.
69. Lundblad, V., and Blackburn, E.H. (1993). An alternative pathway for yeast telomere maintenance rescues est1- senescence. *Cell* *73*, 347-360.
70. Lydeard, J.R., Jain, S., Yamaguchi, M., and Haber, J.E. (2007). Break-induced replication and telomerase-independent telomere maintenance require Pol32. *Nature* *448*, 820-823.
71. Malkova, A., Ivanov, E.L., and Haber, J.E. (1996). Double-strand break repair in the absence of RAD51 in yeast: a possible role for break-induced DNA replication. *Proc Natl Acad Sci U S A* *93*, 7131-7136.
72. Malkova, A., Signon, L., Schaefer, C.B., Naylor, M.L., Theis, J.F., Newlon, C.S., and Haber, J.E. (2001). RAD51-independent break-induced replication to repair a broken chromosome depends on a distant enhancer site. *Genes & development* *15*, 1055-1060.

73. Marciniak, R.A., Cavazos, D., Montellano, R., Chen, Q., Guarente, L., and Johnson, F.B. (2005). A novel telomere structure in a human alternative lengthening of telomeres cell line. *Cancer Res* 65, 2730-2737.
74. Martens, U.M., Chavez, E.A., Poon, S.S., Schmoor, C., and Lansdorp, P.M. (2000). Accumulation of short telomeres in human fibroblasts prior to replicative senescence. *Exp Cell Res* 256, 291-299.
75. Mazon, G., Mimitou, E.P., and Symington, L.S. (2010). SnapShot: Homologous recombination in DNA double-strand break repair. *Cell* 142, 646, 646 e641.
76. McEachern, M.J., and Haber, J.E. (2006). Break-induced replication and recombinational telomere elongation in yeast. *Annual review of biochemistry* 75, 111-135.
77. McIlwraith, M.J., and West, S.C. (2008). DNA repair synthesis facilitates RAD52-mediated second-end capture during DSB repair. *Molecular cell* 29, 510-516.
78. Mine-Hattab, J., and Rothstein, R. (2012). Increased chromosome mobility facilitates homology search during recombination. *Nature cell biology* 14, 510-517.
79. Molenaar, C., Wiesmeijer, K., Verwoerd, N.P., Khazen, S., Eils, R., Tanke, H.J., and Dirks, R.W. (2003). Visualizing telomere dynamics in living mammalian cells using PNA probes. *EMBO J* 22, 6631-6641.
80. Moynahan, M.E., and Jasin, M. (2010). Mitotic homologous recombination maintains genomic stability and suppresses tumorigenesis. *Nature reviews Molecular cell biology* 11, 196-207.

81. Nabetani, A., Yokoyama, O., and Ishikawa, F. (2004). Localization of hRad9, hHus1, hRad1, and hRad17 and caffeine-sensitive DNA replication at the alternative lengthening of telomeres-associated promyelocytic leukemia body. *The Journal of biological chemistry* 279, 25849-25857.
82. Natarajan, S., and McEachern, M.J. (2002). Recombinational telomere elongation promoted by DNA circles. *Mol Cell Biol* 22, 4512-4521.
83. Neale, M.J., and Keeney, S. (2006). Clarifying the mechanics of DNA strand exchange in meiotic recombination. *Nature* 442, 153-158.
84. O'Sullivan, R.J., Arnoult, N., Lackner, D.H., Oganessian, L., Haggblom, C., Corpet, A., Almouzni, G., and Karlseder, J. (2014). Rapid induction of alternative lengthening of telomeres by depletion of the histone chaperone ASF1. *Nature structural & molecular biology* 21, 167-174.
85. Oza, P., Jaspersen, S.L., Miele, A., Dekker, J., and Peterson, C.L. (2009). Mechanisms that regulate localization of a DNA double-strand break to the nuclear periphery. *Genes & development* 23, 912-927.
86. Palm, W., and de Lange, T. (2008). How shelterin protects mammalian telomeres. *Annual review of genetics* 42, 301-334.
87. Perrem, K., Colgin, L.M., Neumann, A.A., Yeager, T.R., and Reddel, R.R. (2001). Coexistence of alternative lengthening of telomeres and telomerase in hTERT-transfected GM847 cells. *Mol Cell Biol* 21, 3862-3875.

88. Petukhova, G.V., Pezza, R.J., Vanevski, F., Ploquin, M., Masson, J.Y., and Camerini-Otero, R.D. (2005). The Hop2 and Mnd1 proteins act in concert with Rad51 and Dmc1 in meiotic recombination. *Nature structural & molecular biology* *12*, 449-453.
89. Petukhova, G.V., Romanienko, P.J., and Camerini-Otero, R.D. (2003). The Hop2 protein has a direct role in promoting interhomolog interactions during mouse meiosis. *Developmental cell* *5*, 927-936.
90. Pezza, R.J., Camerini-Otero, R.D., and Bianco, P.R. (2010). Hop2-Mnd1 condenses DNA to stimulate the synapsis phase of DNA strand exchange. *Biophysical journal* *99*, 3763-3772.
91. Pezza, R.J., Petukhova, G.V., Ghirlando, R., and Camerini-Otero, R.D. (2006). Molecular activities of meiosis-specific proteins Hop2, Mnd1, and the Hop2-Mnd1 complex. *The Journal of biological chemistry* *281*, 18426-18434.
92. Pezza, R.J., Voloshin, O.N., Vanevski, F., and Camerini-Otero, R.D. (2007). Hop2/Mnd1 acts on two critical steps in Dmc1-promoted homologous pairing. *Genes & development* *21*, 1758-1766.
93. Potts, P.R., and Yu, H. (2007). The SMC5/6 complex maintains telomere length in ALT cancer cells through SUMOylation of telomere-binding proteins. *Nature structural & molecular biology* *14*, 581-590.
94. Qi, Z., Redding, S., Lee, J.Y., Gibb, B., Kwon, Y., Niu, H., Gaines, W.A., Sung, P., and Greene, E.C. (2015). DNA sequence alignment by microhomology sampling during homologous recombination. *Cell* *160*, 856-869.

95. Renkawitz, J., Lademann, C.A., and Jentsch, S. (2014). Mechanisms and principles of homology search during recombination. *Nature reviews Molecular cell biology* *15*, 369-383.
96. Robertson, R.B., Moses, D.N., Kwon, Y., Chan, P., Chi, P., Klein, H., Sung, P., and Greene, E.C. (2009). Structural transitions within human Rad51 nucleoprotein filaments. *Proceedings of the National Academy of Sciences of the United States of America* *106*, 12688-12693.
97. Roukos, V., Voss, T.C., Schmidt, C.K., Lee, S., Wangsa, D., and Misteli, T. (2013). Spatial dynamics of chromosome translocations in living cells. *Science* *341*, 660-664.
98. Saleh-Gohari, N., Bryant, H.E., Schultz, N., Parker, K.M., Cassel, T.N., and Helleday, T. (2005). Spontaneous homologous recombination is induced by collapsed replication forks that are caused by endogenous DNA single-strand breaks. *Molecular and cellular biology* *25*, 7158-7169.
99. Sanjana, N.E., Shalem, O., and Zhang, F. (2014). Improved vectors and genome-wide libraries for CRISPR screening. *Nature methods* *11*, 783-784.
100. Saxton, M.J. (2007). A biological interpretation of transient anomalous subdiffusion. I. Qualitative model. *Biophysical journal* *92*, 1178-1191.
101. Schwartzenuber, J., Korshunov, A., Liu, X.Y., Jones, D.T., Pfaff, E., Jacob, K., Sturm, D., Fontebasso, A.M., Quang, D.A., Tonjes, M., *et al.* (2012). Driver mutations in histone H3.3 and chromatin remodelling genes in paediatric glioblastoma. *Nature* *482*, 226-231.

102. Sfeir, A., and de Lange, T. (2012). Removal of shelterin reveals the telomere end-protection problem. *Science* *336*, 593-597.
103. Shanbhag, N.M., Rafalska-Metcalf, I.U., Balane-Bolivar, C., Janicki, S.M., and Greenberg, R.A. (2010). ATM-dependent chromatin changes silence transcription in cis to DNA double-strand breaks. *Cell* *141*, 970-981.
104. Shechter, D., Costanzo, V., and Gautier, J. (2004). ATR and ATM regulate the timing of DNA replication origin firing. *Nature cell biology* *6*, 648-655.
105. Signon, L., Malkova, A., Naylor, M.L., Klein, H., and Haber, J.E. (2001). Genetic requirements for RAD51- and RAD54-independent break-induced replication repair of a chromosomal double-strand break. *Molecular and cellular biology* *21*, 2048-2056.
106. Sorensen, C.S., and Syljuasen, R.G. (2012). Safeguarding genome integrity: the checkpoint kinases ATR, CHK1 and WEE1 restrain CDK activity during normal DNA replication. *Nucleic acids research* *40*, 477-486.
107. Stark, J.M., Hu, P., Pierce, A.J., Moynahan, M.E., Ellis, N., and Jasin, M. (2002). ATP hydrolysis by mammalian RAD51 has a key role during homology-directed DNA repair. *The Journal of biological chemistry* *277*, 20185-20194.
108. Symington, L.S. (2014). End resection at double-strand breaks: mechanism and regulation. *Cold Spring Harbor perspectives in biology* *6*.
109. Tang, J., Cho, N.W., Cui, G., Manion, E.M., Shanbhag, N.M., Botuyan, M.V., Mer, G., and Greenberg, R.A. (2013). Acetylation limits 53BP1 association with

- damaged chromatin to promote homologous recombination. *Nature structural & molecular biology* 20, 317-325.
110. Teng, S.C., and Zakian, V.A. (1999). Telomere-telomere recombination is an efficient bypass pathway for telomere maintenance in *Saccharomyces cerevisiae*. *Molecular and cellular biology* 19, 8083-8093.
111. Thevenaz, P., Ruttimann, U.E., and Unser, M. (1998). A pyramid approach to subpixel registration based on intensity. *IEEE transactions on image processing : a publication of the IEEE Signal Processing Society* 7, 27-41.
112. Toledo, L.I., Altmeyer, M., Rask, M.B., Lukas, C., Larsen, D.H., Povlsen, L.K., Bekker-Jensen, S., Mailand, N., Bartek, J., and Lukas, J. (2013). ATR prohibits replication catastrophe by preventing global exhaustion of RPA. *Cell* 155, 1088-1103.
113. Tsai, Y.L., Tseng, S.F., Chang, S.H., Lin, C.C., and Teng, S.C. (2002). Involvement of replicative polymerases, Tel1p, Mec1p, Cdc13p, and the Ku complex in telomere-telomere recombination. *Molecular and cellular biology* 22, 5679-5687.
114. Wu, G., Jiang, X., Lee, W.H., and Chen, P.L. (2003). Assembly of functional ALT-associated promyelocytic leukemia bodies requires Nijmegen Breakage Syndrome 1. *Cancer research* 63, 2589-2595.
115. Yeager, T.R., Neumann, A.A., Englezou, A., Huschtscha, L.I., Noble, J.R., and Reddel, R.R. (1999). Telomerase-negative immortalized human cells contain a novel type of promyelocytic leukemia (PML) body. *Cancer research* 59, 4175-4179.
116. Zhong, Z.H., Jiang, W.Q., Cesare, A.J., Neumann, A.A., Wadhwa, R., and Reddel, R.R. (2007). Disruption of telomere maintenance by depletion of the

MRE11/RAD50/NBS1 complex in cells that use alternative lengthening of telomeres.

The Journal of biological chemistry 282, 29314-29322.